

The Recent Evolution of a Symbiotic Ion Channel in the Legume Family Altered Ion Conductance and Improved Functionality in Calcium Signaling

Muthusubramanian Venkateshwaran,^{a,1} Ana Cosme,^{b,1} Lu Han,^c Mari Banba,^c Kenneth A. Satyshur,^d Enrico Schleiff,^e Martin Parniske,^b Haruko Imaizumi-Anraku,^c and Jean-Michel Ané^{a,2}

^aDepartment of Agronomy, University of Wisconsin, Madison, Wisconsin 53706

^bLudwig-Maximilians-Universität München, Faculty of Biology, Genetics, 82152 Martinsried, Germany

^cDivision of Plant Sciences, National Institute of Agrobiological Sciences, Tsukuba, Ibaraki 305-8602, Japan

^dUniversity of Wisconsin Carbone Cancer Center, School of Medicine and Public Health, University of Wisconsin, Madison, Wisconsin 53705

^eGoethe University, Biozentrum, 60438 Frankfurt, Germany

Arbuscular mycorrhiza and the rhizobia-legume symbiosis are two major root endosymbioses that facilitate plant nutrition. In *Lotus japonicus*, two symbiotic cation channels, CASTOR and POLLUX, are indispensable for the induction of nuclear calcium spiking, one of the earliest plant responses to symbiotic partner recognition. During recent evolution, a single amino acid substitution in DOES NOT MAKE INFECTIONS1 (DMI1), the POLLUX putative ortholog in the closely related *Medicago truncatula*, rendered the channel solo sufficient for symbiosis; *castor*, *pollux*, and *castor pollux* double mutants of *L. japonicus* were rescued by *DMI1* alone, while both Lj-CASTOR and Lj-POLLUX were required for rescuing a *dmi1* mutant of *M. truncatula*. Experimental replacement of the critical serine by an alanine in the selectivity filter of Lj-POLLUX conferred a symbiotic performance indistinguishable from DMI1. Electrophysiological characterization of DMI1 and Lj-CASTOR (wild-type and mutants) by planar lipid bilayer experiments combined with calcium imaging in Human Embryonic Kidney-293 cells expressing DMI1 (the wild type and mutants) suggest that the serine-to-alanine substitution conferred reduced conductance with a long open state to DMI1 and improved its efficiency in mediating calcium oscillations. We propose that this single amino acid replacement in the selectivity filter made DMI1 solo sufficient for symbiosis, thus explaining the selective advantage of this allele at the mechanistic level.

INTRODUCTION

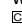
The majority of land plants develop arbuscular mycorrhiza (AM) for improved nutrient uptake and protection against stresses (Akiyama et al., 2005). On the other hand, root nodule (RN) symbiosis, established between legume and rhizobia, results in the formation of nitrogen-fixing RNs (Venkateshwaran and Ané, 2011). The development of root endosymbioses is coordinated by signal exchanges between plants and their microbial symbionts. Rhizobia produce diffusible lipochitooligosaccharidic signals, Nod factors (Dénarié et al., 1996). Similarly, AM fungi produce diffusible signals called Myc factors (Akiyama et al., 2005; Maillet et al., 2011; Mukherjee and Ané, 2011). Perception of Nod or Myc factors initiates early symbiotic responses in host plants, such as calcium (Ca²⁺) spiking and symbiotic gene expression (Ehrhardt et al., 1996; Wais et al., 2000, 2002; Riely

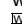
et al., 2006; Sieberer et al., 2009; Chabaud et al., 2011). Although RN and AM are distinct symbioses, they require a common set of genes in host plants to support rhizobial and fungal infections. Genetic studies in legumes such as *Medicago truncatula*, *Lotus japonicus*, and pea (*Pisum sativum*) have identified several common symbiosis genes. Several genes that play crucial roles in both RN and AM symbioses have been identified so far in model legumes (Kistner et al., 2005; Groth et al., 2010; Maillet et al., 2011; Murray et al., 2011). Among them, *M. truncatula* DOES NOT MAKE INFECTIONS1 (*DMI1*) and *L. japonicus* CASTOR and POLLUX encode nuclear ion channels that are required for the initiation of Nod and Myc factor-induced Ca²⁺ spiking (Ané et al., 2002, 2004; Imaizumi-Anraku et al., 2005; Peiter et al., 2007; Riely et al., 2007; Charpentier et al., 2008; Kosuta et al., 2008; Capoen et al., 2011). *M. truncatula* DMI1 and pea DMI1 aka SYMBIOSIS8 (*SYM8*) are putative orthologs of Lj-POLLUX and putative paralogs of Lj-CASTOR (Zhu et al., 2006; Edwards et al., 2007). *SYM8* can functionally substitute DMI1 in *M. truncatula* (Edwards et al., 2007). These DMI1 homologs are present throughout land plants and represent ancient innovations that probably allowed the development of the AM symbiosis and colonization of land by plants (Zhu et al., 2006; Wang et al., 2010). Consistent with the phylogenetically widespread occurrence of common symbiosis genes and AM, rice (*Oryza sativa*) putative orthologs Os-CASTOR and Os-POLLUX are required for the AM symbiosis (Banba et al., 2008; Gutjahr

¹ These authors contributed equally to this work.

² Address correspondence to jane@wisc.edu.

The author responsible for distribution of materials integral to the findings presented in this article in accordance with the policy described in the Instructions for Authors (www.plantcell.org) is: Jean-Michel Ané (jane@wisc.edu).

 Some figures in this article are displayed in color online but in black and white in the print edition.

 Online version contains Web-only data.

www.plantcell.org/cgi/doi/10.1105/tpc.112.098475

et al., 2008; Chen et al., 2009). The presence of a *POLLUX* putative ortholog in *Arabidopsis thaliana* is intriguing, as *Arabidopsis* does not undergo mycorrhization. Therefore, it has been hypothesized that At-*POLLUX* might play a nonsymbiotic role.

L. japonicus *CASTOR* and *POLLUX* are nonselective ion channels with a preference for K⁺ over anions (Charpentier et al., 2008). Competition experiments with Lj-*CASTOR* reconstituted in planar lipid bilayers revealed a preference for K⁺ over other cations, such as Na⁺ and Ca²⁺. Unfortunately, Lj-*POLLUX* was not amenable to lipid bilayer analysis but was able to complement a K⁺ transport-deficient yeast mutant, suggesting its ability to conduct K⁺ (Charpentier et al., 2008). Although Lj-*CASTOR* and Lj-*POLLUX* reside on the nuclear envelope and perform similar roles in symbiotic signaling, these two proteins do not appear to interact and form exclusively homomeric ion channels (Charpentier et al., 2008). While both *CASTOR* and *POLLUX* are indispensable for symbiotic signaling in *L. japonicus*, *POLLUX* putative orthologs *DMI1* and *SYM8* seem to function alone in *M. truncatula* and pea, respectively. Although more than 30 *castor* mutant alleles have been identified in *L. japonicus*, no *castor* mutant has been found so far in *M. truncatula* (Perry et al., 2009). Likewise, despite multiple screens for nodulation-defective pea mutants, no *CASTOR* ortholog has been identified through forward genetics in *P. sativum*.

Here, we show that *DMI1* in the Viciae and Trifolieae legume tribes has evolved to take over the role of both *POLLUX* and *CASTOR*, decreasing drastically the functional importance of *CASTOR* in these tribes. Site-directed mutagenesis experiments revealed that a single Ser-to-Ala substitution in the filter region of *DMI1* is responsible for its neofunctionality. Furthermore, planar lipid bilayer experiments with *DMI1* and Lj-*CASTOR* (the wild type and a mutant that mimics the filter region of *DMI1*) indicated that this Ser-to-Ala substitution in the filter confers a reduced conductance to *DMI1*. Together, our data reveal an unexpected twist in the evolution of ancestral and essential symbiotic proteins and highlight a single mutation responsible for the functional improvement of *DMI1* for RN and AM symbioses.

RESULTS

Legume Nodulation and AM Are Independent of *CASTOR* in *M. truncatula*

The predicted structure of Mt-*CASTOR* (824 amino acids) comprises a nuclear localization signal in the N terminus, followed by four transmembrane domains and a soluble region with an RCK (for regulator of conductance of K⁺) domain, which is highly similar to MthK, a bacterial Ca²⁺-gated potassium channel (Imaizumi-Anraku et al., 2005). The pore region, including a characteristic pore helix, filter, and hinge, is located between the third and fourth transmembrane domains (see Supplemental Figure 1 online). We searched for Mt-*CASTOR* mutants in the TILLING or *Tnt1* insertion libraries without success (Tadege et al., 2005, 2008). Since no mutant was available for functional studies, we used an RNA interference (RNAi)-based gene silencing strategy to investigate its role in RN and

AM. As a positive control, we targeted the well-characterized symbiotic gene *DMI1*. As expected, this resulted in a decline of nodule numbers in *DMI1-RNAi*-expressing transgenic roots (Figure 1A). The Mt-*CASTOR-RNAi* transgenic roots showed a significant reduction in Mt-*CASTOR* expression at the transcript level over control roots transformed with an empty vector (see Supplemental Figure 2A online). However, there was no significant reduction in the nodule number in Mt-*CASTOR-RNAi*-expressing transgenic roots (Figure 1A). These results indicate that the RNAi-based gene silencing strategy was efficient and that Mt-*CASTOR*, compared with *DMI1*, plays a less significant role, if any, in RN symbiosis. In the case of AM symbiosis, Mt-*CASTOR-RNAi* roots, as well as control roots, showed normal AM associations with intracellular hyphae and arbuscules (Figure 1B). To quantify the abundance of arbuscules in Mt-*CASTOR-RNAi* and control roots, we performed RT-PCR to monitor the expression level of *M. truncatula phosphate transporter4* (Mt-*PT4*). Mt-*PT4* expression is induced only upon arbuscule formation and exclusively in arbuscule-containing cells, and its expression level positively correlates with the degree of AM colonization and arbuscule formation (Harrison et al., 2002). Hence, we used this marker to quantify the arbuscule abundance in Mt-*CASTOR-RNAi* and control roots. We showed that the expression level of Mt-*PT4* upon AM colonization is similar in Mt-*CASTOR-RNAi* roots to that of control roots (Figure 1C; see Supplemental Figure 2B online), suggesting that silencing Mt-*CASTOR* does not affect AM colonization. Furthermore, Mt-*CASTOR* failed to rescue two alleles of Lj-*castor* mutants; Lj-*castor-4* (see Supplemental Figure 3A online; Table 1), Lj-*castor-8* (Table 1), Lj-*pollux*, and the Lj-*castor pollux* double mutant (see Supplemental Figures 3B and 3C online; Table 1). Taken together, these observations demonstrate that Mt-*CASTOR* does not play a significant role in RN and AM symbioses.

DMI1 and *SYM8* Acquired a Refined Role in Symbiotic Signaling

The previous observations suggest a reduced importance of Mt-*CASTOR* in both RN and AM symbioses. We therefore investigated whether *DMI1* can indeed mediate symbiotic signaling alone. To compare the symbiotic functionality of *DMI1* and Lj-*POLLUX*, we performed a series of cross-species rescue experiments. In transgenic root assays, Lj-*CASTOR* could fully rescue Lj-*castor* mutants and mature nodules were formed, whereas Lj-*CASTOR* failed to rescue Lj-*pollux* and Lj-*castor pollux* mutations, resulting in the formation of few non-functional immature nodules (bumps) (Figure 2A, Table 1; see Supplemental Figures 3D to 3F online). Similarly, Lj-*POLLUX* could fully rescue an Lj-*pollux* mutation in *L. japonicus*, while a few bumps were formed on Lj-*castor* or Lj-*castor pollux* double mutants (Figure 2B, Table 1; see Supplemental Figures 3G to 3I online).

Lj-*POLLUX* was introduced in three different Lj-*castor* mutant alleles, including total deletion mutants (Lj-*castor-8* and G00532-21), but no nodules formed (Table 1). Interestingly, *DMI1* was able to rescue not only the single mutants of Lj-*castor* and Lj-*pollux*, but also the Lj-*castor pollux* double mutant (Figure

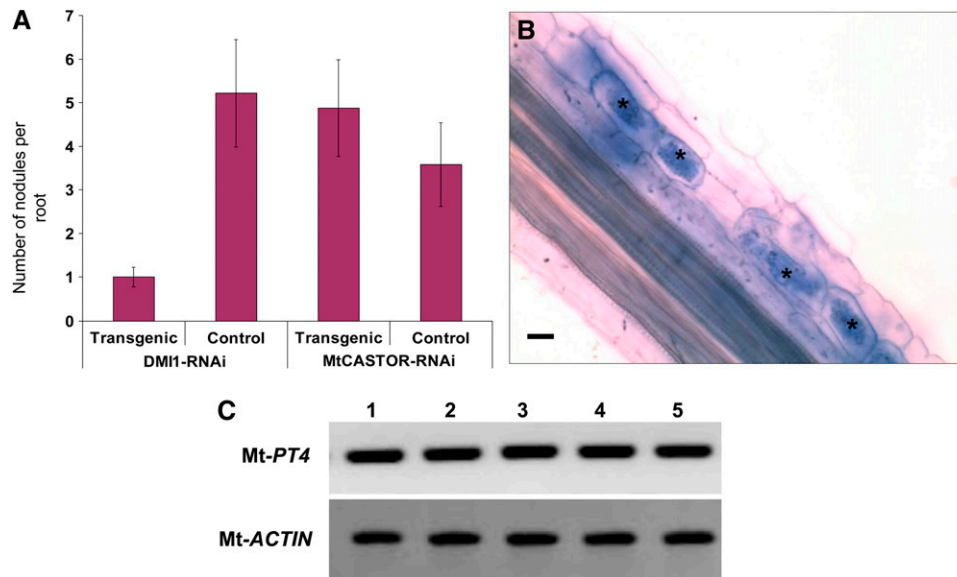


Figure 1. Effect of Mt-CASTOR-RNAi on Nodulation and Arbuscular Mycorrhization in *M. truncatula*.

(A) Reduction in the expression of Mt-CASTOR did not result in a reduction in the nodulation rate when compared with the control empty vector-expressing transgenic roots, whereas reduction in the expression level of *DMI1* (used here as a positive control) resulted in a significant reduction in the nodulation rate when compared with the control empty vector expressing transgenic roots. Data are mean \pm SD ($n = 90$).

(B) Mt-CASTOR-RNAi-expressing transgenic root displaying mycorrhizal association with *G. intraradices*, as is evident from the presence of arbuscules ($n = 36$). Asterisks indicate arbuscules in the root epidermal cells. Bar = 20 μ m.

(C) Analysis of Mt-PT4 expression level in four AM-colonized Mt-CASTOR-RNAi-expressing roots (lanes 1 to 4) and control root (lane 5) by RT-PCR. Each lane represents three technical replicates obtained from one experiment comprising 12 plants each for Mt-CASTOR-RNAi and empty vector control. The experiment was repeated three times; $n = 36$. Mt-Actin was used as a loading control.

[See online article for color version of this figure.]

2C, Table 1; see Supplemental Figures 3J to 3L online). The Lj-*castor pollux* double mutant transformed with *DMI1* was also colonized by *Glomus intraradices*, as indicated by the formation of arbuscules and vesicles (see Supplemental Figure 4A online). Like *DMI1*, *SYM8* was also able to rescue the nodulation phenotype in Lj-*castor*, Lj-*pollux*, and Lj-*castor pollux* mutants (see Supplemental Figures 3M to 3O online). These results indicate that DMI1 putative orthologs in *M. truncatula* and pea have the capacity to compensate for the loss of both CASTOR and POLLUX ion channels in *L. japonicus* in both RN and AM symbioses.

Lj-CASTOR and POLLUX Share Their Symbiotic Function Nonredundantly

In agreement with an acquired neofunctionality of DMI1, Lj-CASTOR and POLLUX failed to fully rescue *dmi1-4* when expressed individually. This failure was observed regardless of whether their expression was controlled by their respective native promoters (Lj-CASTOR_{pro} or Lj-POLLUX_{pro}), constitutive promoters (cauliflower mosaic virus 35S_{pro} or Lj Ubq1_{pro}), or even the native promoter of *DMI1* (DMI1_{pro}). *Dmi1-4* roots transformed with Lj-CASTOR showed absolutely no response to inoculation with *Sinorhizobium meliloti* (pXLGD4) (Figure 3A, Table 2). Lj-POLLUX-transformed *dmi1-4* roots showed only bumps (Figure 3B; Table 2). These nodule bumps were small,

pale, and devoid of bacteria, as no β -galactosidase activity (due to *hema*_{pro}:*lacZ*) was detected (see Supplemental Figures 5A and 5C online). However, when coexpressed, Lj-CASTOR and Lj-POLLUX rescued the *dmi1-4* mutant, leading to the formation of colonized and functional nodules in which *nifH* expression (*nifH*_{pro}:*uidA*) was detected (Bright et al., 2005) (Figure 3C, Table 2; Supplemental Figures 6B and 6E online). Expression of Lj-CASTOR and Lj-POLLUX in these double transgenic roots was confirmed at the transcript level by RT-PCR (see Supplemental Figure 2C online). Coexpression of Lj-CASTOR and Lj-POLLUX in *dmi1-4* roots also restored mycorrhization, accompanied by the development of arbuscules and vesicles and expression of Mt-PT4 (see Supplemental Figures 4B and 4D online). As a control, *DMI1*, expressed under the control of 35S_{pro} or its own promoter, was able to rescue fully the *dmi1-4* mutant (Figure 3D, Table 2). Collectively, our results indicate that CASTOR and POLLUX are both required in *L. japonicus*, while DMI1 (from *M. truncatula* or pea) can compensate for the loss of both CASTOR and POLLUX.

A Ser-to-Ala Substitution in the Filter Region of DMI1 Is Sufficient for Its Integrated Function

We sought to identify the determinants responsible for the neofunctionality of DMI1 and SYM8. We noticed a single amino acid difference in the predicted filter region of DMI1 and SYM8

Table 1. Summary of Rescue Assay Performed with Different Constructs Expressing *DMI1*, Lj-CASTOR, Lj-POLLUX, Lj-CASTOR^{S266A}, Lj-POLLUX^{S329A}, and *DMI1*^{A294S} in *castor*, *pollux*, and *castor pollux* Double Mutants of *L. japonicus*

Mutant Line	Construct	Nodulated Plants/Total Plants (Bump-Forming Plants/Total Plants)
Lj- <i>castor</i> -4	35S _{pro} :DMI1	69/70
Lj- <i>pollux</i> -2	35S _{pro} :DMI1	67/70
Lj- <i>caspol</i> ^a	35S _{pro} :DMI1	56/65
Lj- <i>castor</i> -4	35S _{pro} :Mt-CASTOR	0/30
Lj- <i>castor</i> -8 ^b	35S _{pro} :Mt-CASTOR	0/13
Lj- <i>pollux</i> -2	35S _{pro} :Mt-CASTOR	0/31
Lj- <i>caspol</i>	35S _{pro} :Mt-CASTOR	0/16
Lj- <i>castor</i> -4	35S _{pro} :Lj-CASTOR	26/29
Lj- <i>castor</i> -8	35S _{pro} :Lj-CASTOR	34/41
G00532-21 ^b	35S _{pro} :Lj-CASTOR	16/19
Lj- <i>pollux</i> -2	35S _{pro} :Lj-CASTOR	0/24 (1/24)
Lj- <i>caspol</i>	35S _{pro} :Lj-CASTOR	0/55 (3/55)
Lj- <i>castor</i> -4	35S _{pro} :Lj-POLLUX	0/18 (4/18)
Lj- <i>castor</i> -8	35S _{pro} :Lj-POLLUX	0/31
G00532-21	35S _{pro} :Lj-POLLUX	0/18
Lj- <i>pollux</i> -2	35S _{pro} :Lj-POLLUX	18/20
Lj- <i>caspol</i>	35S _{pro} :Lj-POLLUX	0/37 (1/37)
Lj- <i>caspol</i>	35S _{pro} :GFP	0/34
Lj- <i>castor</i> -4	35S _{pro} :Lj-CASTOR ^{S266A}	20/24
Lj- <i>pollux</i> -2	35S _{pro} :Lj-CASTOR ^{S266A}	0/23
Lj- <i>caspol</i>	35S _{pro} :Lj-CASTOR ^{S266A}	0/21
Lj- <i>castor</i> -4	35S _{pro} :Lj-POLLUX ^{S329A}	16/25
Lj- <i>pollux</i> -2	35S _{pro} :Lj-POLLUX ^{S329A}	17/19
Lj- <i>caspol</i>	35S _{pro} :Lj-POLLUX ^{S329A}	8/10
Lj- <i>castor</i> -4	35S _{pro} :DMI1 ^{A294S}	1/47
Lj- <i>pollux</i> -2	35S _{pro} :DMI1 ^{A294S}	0/39
Lj- <i>caspol</i>	35S _{pro} :DMI1 ^{A294S}	0/51
Lj- <i>castor</i> -4	35S _{pro} :SYM8 (genome)	45/45
Lj- <i>pollux</i> -2	35S _{pro} :SYM8 (genome)	42/46
Lj- <i>caspol</i>	35S _{pro} :SYM8 (genome)	52/52
Lj- <i>castor</i> -4	35S _{pro} :SYM8 (cDNA)	17/17
Lj- <i>pollux</i> -2	35S _{pro} :SYM8 (cDNA)	18/19
Lj- <i>caspol</i>	35S _{pro} :SYM8 (cDNA)	22/22

^aLj-*castor pollux* double mutant is derived from the cross between Lj-*castor*-5 and Lj-*pollux*-2 alleles.

^bLj-*castor*-8 and another Lj-*castor* allele G00532-21 completely lack the genomic region of Lj CASTOR.

when compared with the filter region of Lj-CASTOR, Lj-POLLUX, and Mt-CASTOR. The selectivity filters of DMI1 and SYM8 are composed of the amino acid residues ADAGNHA, and these two putative orthologs mutually rescue each other (Edwards et al., 2007). Lj-CASTOR and Lj-POLLUX have ADAGNHA as a filter region, in which an Ala is substituted by a Ser. The filter region of Lj-CASTOR and Lj-POLLUX was therefore changed to ADAGNHA and that of DMI1 to ADAGNHA through site-directed mutagenesis. The modified Lj-CASTOR^{S266A}, Lj-POLLUX^{S329A}, and *DMI1*^{A294S} were tested in rescue assays. Lj-CASTOR^{S266A} retained the ability to rescue the Lj-*castor* mutant (Table 1), while it failed to rescue the Lj-*pollux*, Lj-*castor pollux*, and *dmi1* mutants (Figure 2D, Tables 1 and 2).

By contrast, Lj-POLLUX^{S329A} showed striking differences in its functionality. Lj-POLLUX^{S329A} not only restored nodulation in Lj-*pollux*, but also in Lj-*castor* and Lj-*castor pollux* double mutants, similar to *DMI1* (Figure 2E, Table 1). In addition, when expressed alone, Lj-POLLUX^{S329A} rescued *dmi1* mutations in *M.*

truncatula even in the absence of Lj-CASTOR (Figure 3E, Table 2). Roots of *dmi1-4* transformed with Lj-POLLUX^{S329A} developed arbuscules and vesicles (see Supplemental Figure 4C online), expressed Mt-PT4 upon inoculation with *G. intraradices* (see Supplemental Figure 4D online), and developed mature functional nodules (see Supplemental Figures 6C and 6F online) upon inoculation with *S. melloti*. These observations indicate that the S329A mutation in the filter region of Lj-POLLUX was sufficient to confer the ability of this modified Lj-POLLUX to act solely in both *L. japonicus* and *M. truncatula*.

The reciprocal mutation in DMI1 (*DMI1*^{A294S}) altered its functionality in rescue assays. *DMI1*^{A294S} failed to rescue Lj-*castor*, Lj-*pollux*, and Lj-*castor pollux* mutants (Figure 2F, Table 1). However, *DMI1*^{A294S} was able to rescue a *dmi1* null mutant in *M. truncatula*, in which the expression of Mt-CASTOR was unaltered (Table 2). However, when Mt-CASTOR expression was reduced by the introduction of the Mt-CASTOR-RNAi construct, *DMI1*^{A294S} did not rescue *dmi1* in *M. truncatula* (Figure 3F, Table

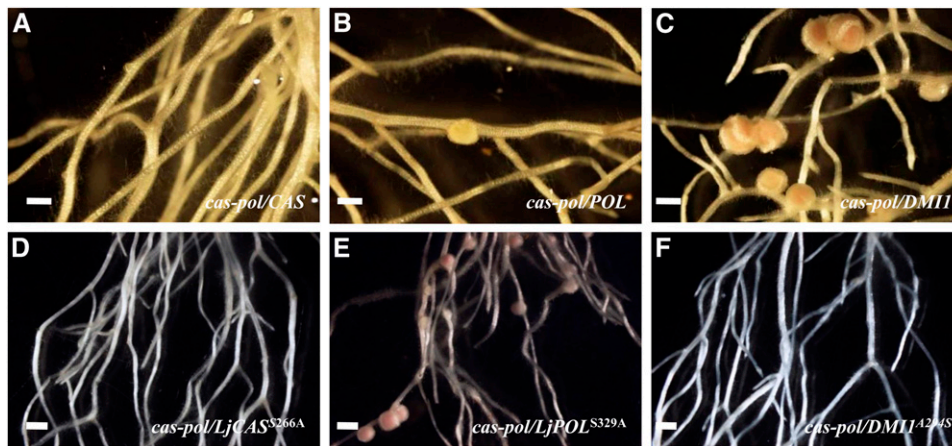


Figure 2. Rescue Assays in *L. japonicus* Mutants with Lj-CASTOR, Lj-POLLUX, *DMI1*, and Modified Alleles.

(A) to (C) Rescue of the *L. japonicus castor pollux* double mutant by Lj-CASTOR, Lj-POLLUX, and *DMI1*.

(A) Lj-CASTOR rescued only *castor* but failed to rescue the Lj-*castor pollux* double mutant.

(B) Lj-POLLUX rescued only Lj-*pollux* but failed to rescue the Lj-*castor pollux* double mutant.

(C) *DMI1* rescues both single and double mutant Lj-*castor pollux*.

(D) to (F) Rescue of *L. japonicus castor pollux* double mutant by Lj-CASTOR^{S266A}, Lj-POLLUX^{S329A}, and *DMI1*^{A294S}.

(D) Lj-CASTOR^{S266A} rescues only Lj-*castor*.

(E) Lj-POLLUX^{S329A} gains function and rescues single as well as double mutant Lj-*castor pollux*.

(F) *DMI1*^{A294S} loses function and fails to rescue the Lj-*castor pollux* mutant.

In the figures, lowercase, italicized words correspond to the mutant line and uppercase, italicized words correspond to the respective gene or modified allele used for the rescue assay. Bars = 2 mm.

[See online article for color version of this figure.]

2), and only bumps formed that were devoid of rhizobia inside nodules. As a control, wild-type *DMI1* was able to restore nodulation in the *dmi1-4* mutant line expressing Mt-CASTOR-RNAi (Table 2). Hence, this Ala-to-Ser mutation in *DMI1* caused a functional dependency of the modified *DMI1* on Mt-CASTOR. These results demonstrate that the Ser/Ala polymorphism in the filter region of these ion channels is the major determinant for the neofunctionality of *DMI1*.

Impact of Ser-to-Ala Substitution on a Nonlegume *DMI1* Ortholog

The Ser-to-Ala substitution in the filter region also has significant impact on *DMI1* putative orthologs of nonleguminous plants. The nonmycorrhizal plant, *Arabidopsis*, encodes a *POLLUX* putative ortholog, which contains the amino acid sequence ADGSHA with one additional polymorphism, Asn/Ser, in its selectivity filter. At-*POLLUX* fails to rescue the *dmi1-4* mutant, while the introduction of an equivalently positioned Ser-to-Ala substitution enables At-*POLLUX*^{S237A} to rescue the *dmi1-4* mutant (Table 2). At-*POLLUX*^{S237A S239N}, which includes an additional Asn-to-Ser substitution, also rescues the *dmi1-4* mutant, similar to At-*POLLUX*^{S237A}, indicating that the Ser-to-Ala substitution is sufficient to confer improved function to At-*POLLUX* (Table 2). Considering that the overall sequence similarity between At-*POLLUX* and *DMI1* is only 67%, this result confirms that the Ser/Ala polymorphism in the filter region is the key determinant for the symbiotic capability of the *DMI1* and *POLLUX* channels.

Tracing the Ser-to-Ala Substitution of *DMI1* Homologs in Legumes

Amino acid sequences at the pore region of *DMI1* homologs were obtained from 20 legume genera largely representing Caesalpinioideae (*Cercis*), Genistoid (*Lupinus*), Dalbergioideae (*Arachis*), Milletoideae (*Cajanus*, *Glycine*, *Vigna*, and *Phaseolus*), Robinioideae (*Lotus*), Galegoideae (*Astragalus* and *Galega*), and Vicioideae (*Cicer*, *Ononis*, *Medicago*, *Trigonella*, *Mellilotus*, *Trifolium*, *Pisum*, *Lathyrus*, *Vicia*, and *Lens*). The filter sequence ADGSHA was observed among *POLLUX* putative orthologs from Caesalpinioideae, Genistoid, Dalbergioideae, Milletoideae, Robinioideae, and Galegoideae and in a few members of Vicioideae (*Cicer*). The presence of the Ala residue is restricted to the Trifolieae and Vicioideae tribes among the Vicioideae clade and therefore occurred rather recently in legume evolution (Figure 4; see Supplemental Data Set 1 online).

The Ser-to-Ala Substitution in the Filter of *DMI1* Reduces Potassium Conductance

We hypothesized that the Ser-to-Ala substitution in the filter region alters the ion permeation of *DMI1* and *SYM8* when compared with Lj-CASTOR and Lj-POLLUX. To test this hypothesis, the effect of this substitution was analyzed by comparing *DMI1* with Lj-CASTOR and Lj-CASTOR carrying the Ser-to-Ala substitution (Lj-CASTOR^{S266A}), which mimics the filter region of *DMI1*. Lj-CASTOR was chosen for these experiments because its filter region sequence is identical to that

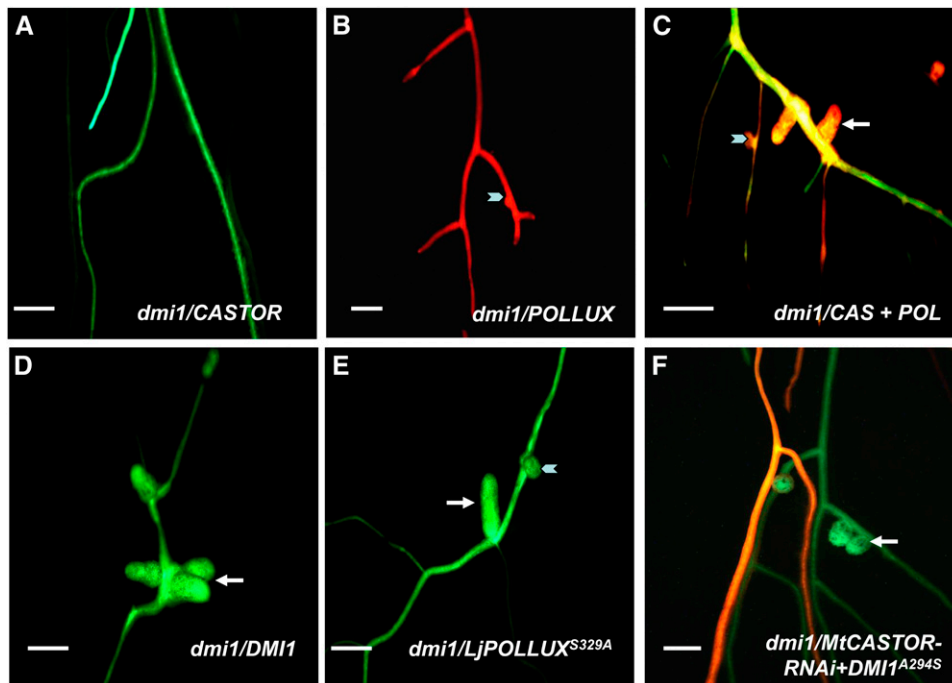


Figure 3. Rescue Assays in *M. truncatula dmi1* Mutant with Lj-CASTOR, Lj-POLLUX, *DMI1*, and Modified Alleles.

(A) to (C) Rescue of the *M. truncatula dmi1* mutation by Lj-CASTOR and Lj-POLLUX.

(A) Lj-CASTOR expressed alone does not rescue nodulation phenotype in *dmi1* when inoculated with *S. meliloti* (pXLGD4).

(B) Lj-POLLUX expressed alone does not rescue nodulation phenotype in *dmi1* mutant as only immature nodules or nodule bumps were observed in few instances.

(C) Lj-CASTOR and Lj-POLLUX together rescue *dmi1* as mature functional nodules were formed.

(D) and (E) Rescue of *M. truncatula dmi1* mutation by *DMI1*, Lj-POLLUX^{S329A}, and *DMI1*^{A294S}.

(D) *DMI1* rescues nodulation phenotype in *dmi1* mutant.

(E) Lj-POLLUX^{S329A} gains function and rescues *dmi1* without Lj-CASTOR.

(F) *DMI1*^{A294S} does not rescue *dmi1* when paired with Mt-CASTOR-RNAi.

Mature nodules are shown by white arrows; nodule bumps are shown by white arrowheads. In (C), the double transgenic roots of *dmi1* line expressing Lj-CASTOR and Lj-POLLUX were colocalized for GFP (for Lj-CASTOR) and DsRED1 (for Lj-POLLUX), yielding yellow to orange fluorescent roots. In (F), the double transgenic roots of *dmi1* line expressing *DMI1*^{A294S} and Mt-CASTOR-RNAi were colocalized for GFP (for *DMI1*^{A294S}) and DsRED1 (for Mt-CASTOR-RNAi), yielding yellow to orange fluorescent roots. In the figures, lowercase, italicized words correspond to the mutant line and uppercase, italicized words correspond to wild-type gene used for rescue assay. Bars = 5 mm.

of Lj-POLLUX and its electrophysiological behavior has already been characterized (Charpentier et al., 2008). Unfortunately, Lj-POLLUX has not been amenable to any patch clamp system tested so far. However, since the filter region is the major determinant of ion selectivity, we used Lj-CASTOR for testing the impact of the Ser-to-Ala mutation in the predicted filter region on the channel properties, and we then compared the two Lj-CASTOR variants with the *DMI1* channel.

Lj-CASTOR has a positive reversal potential in the presence of KCl, indicating permeability to K⁺, and a negative reversal potential in CaCl₂, revealing permeability for the Cl⁻ anion as well (Charpentier et al., 2008). In this study, we show that in symmetrical KCl solution, Lj-CASTOR (ADSGNHA) exhibited a conductance of around 175 pS (Figure 5A). Interestingly, the *DMI1* channel (ADAGNHA) had a much lower conductance of only 64 pS (Figure 5B). Consistent with the idea that the sequence differences in the filter region are responsible for this altered

channel behavior, we observed that Lj-CASTOR^{S266A} with a filter region identical to *DMI1* (ADAGNHA) had a similar low conductance of 61 pS (Figure 5C).

The Ser-to-Ala mutation in the filter region reduces the ion flow without significantly altering the selectivity. Since the filter region is a major determinant of ion permeation, and given that Lj-CASTOR^{S266A} and *DMI1* carrying the same filter region show the same electrophysiological shift relative to the Lj-CASTOR channel, we hypothesize that Lj-POLLUX has a conductance similar to Lj-CASTOR and that this is higher than that of *DMI1*. Thus, our results indicate that the better symbiotic performance of *DMI1*, SYM8, and Lj-POLLUX^{S329A} is associated with a reduction in K⁺ conductance compared with Lj-CASTOR and Lj-POLLUX.

We also measured the mean open time for *DMI1*, Lj-CASTOR, and Lj-CASTOR^{S266A} by pooling single channel currents obtained in symmetrical 250 mM KCl at various voltages. We were able to record and analyze gating events for *DMI1*, Lj-CASTOR,

Table 2. Summary of Rescue Assay Performed with Different Constructs Expressing *DMI1*, *Lj-CASTOR*, *Lj-POLLUX*, *Lj-CASTOR^{S266A}*, *Lj-POLLUX^{S329A}*, and *DMI1^{A294S}* in the *dmi1-4* (GY15-3F-4) Mutant of *M. truncatula*

Construct	Mutant Line	Visible/Selection Marker	Nodulated Plants/Total Plants (Bump-Forming Plants/Total Plants)
<i>35S_{pro}:DMI1</i>	<i>dmi1-4^a</i>	GFP	51/105 (15/105)
<i>DMI1_{pro}:DMI1</i>	<i>dmi1-4</i>	DsRED1	45/89 (9/89)
<i>35S_{pro}:DMI1^{A294S}</i>	<i>dmi1-4</i>	GFP	35/112 (12/112)
<i>35S_{pro}:DMI1^{A294V}</i>	<i>dmi1-4</i>	GFP	0/93
<i>35S_{pro}:DMI1^{A294S} + 35S_{pro}:Mt-CASTOR-RNAi</i>	<i>dmi1-4</i>	GFP + DsRED1	0/36 (21/36)
<i>35S_{pro}:DMI1 + 35S_{pro}:Mt-CASTOR-RNAi</i>	<i>dmi1-4</i>	GFP + DsRED1	20/20
<i>35S_{pro}:Lj-POLLUX</i>	<i>dmi1-4</i>	DsRED1	0/178 (1/178)
<i>Lj-Ubq1_{pro}:Lj-POLLUX</i>	<i>dmi1-4</i>	GFP	0/81 (11/81)
<i>Lj-POLLUX_{pro}:Lj-POLLUX:RFP^b</i>	<i>dmi1-4</i>	Kanamycin	0/143
<i>DMI1_{pro}:Lj-POLLUX</i>	<i>dmi1-4</i>	DsRED1	0/134
<i>35S_{pro}:Lj-POLLUX^{S329A}</i>	<i>dmi1-4</i>	GFP	76/171 (19/171)
<i>35S_{pro}:Lj-CASTOR</i>	<i>dmi1-4</i>	GFP	0/145
<i>Lj-Ubq1_{pro}:Lj-CASTOR</i>	<i>dmi1-4</i>	GFP	0/49
<i>Lj-CASTOR_{pro}:Lj-CASTOR:RFP</i>	<i>dmi1-4</i>	Kanamycin	0/53
<i>DMI1_{pro}:Lj-CASTOR</i>	<i>dmi1-4</i>	GFP	0/81
<i>35S_{pro}:Lj-CASTOR^{S266A}</i>	<i>dmi1-4</i>	DsRED1	0/95
<i>35S_{pro}:Lj-CASTOR + 35S_{pro}:Lj-POLLUX</i>	<i>dmi1-4</i>	GFP + DsRED1	36/59 (13/59)
<i>Lj-Ubq1_{pro}:Lj-CASTOR + Lj-Ubq1_{pro}:Lj-POLLUX</i>	<i>dmi1-4</i>	GFP	55/64 (11/64)
<i>35S_{pro}:Lj-CASTOR^{S266A} + 35S_{pro}:Lj-POLLUX^{S329A}</i>	<i>dmi1-4</i>	GFP + DsRED1	16/28 (3/28)
<i>35S_{pro}:Mt-CASTOR</i>	<i>dmi1-4</i>	GFP	0/102
<i>DMI1_{pro}:Mt-CASTOR</i>	<i>dmi1-4</i>	DsRED1	0/95
<i>35S_{pro}:At-POLLUX(ADSGSHA)</i>	<i>dmi1-4</i>	GFP	0/40
<i>35S_{pro}:At-POLLUX(ADAGSHA)</i>	<i>dmi1-4</i>	GFP	16/36
<i>35S_{pro}:At-POLLUX(ADAGNHA)</i>	<i>dmi1-4</i>	GFP	14/36

^a*dmi1-4* mutant line lacks full-length genomic region of *DMI1*.

^bRFP, red fluorescent protein.

and *Lj-CASTOR^{S266A}* at different voltages (Figure 6; see Supplemental Figure 7 online). The difference in gating kinetics was quantified by open-time histograms of peaking frequencies of *DMI1*, *Lj-CASTOR*, and *Lj-CASTOR^{S266A}* channel open durations at different voltages (Figure 6A). It was interesting to note that *Lj-CASTOR^{S266A}* and *DMI1* channels have a longer open lifetime (59 ± 1 and 16 ± 1 ms, respectively) than *Lj-CASTOR* (4 ± 1 ms) (Figure 6B; see Supplemental Figure 7 online). Our observations suggest that the Ser-to-Ala substitution at the filter region of *DMI1* confers longer open lifetime to the channel in addition to reducing its ion conductance.

Ser-to-Ala Substitution in the Filter Improves the Ca^{2+} -Induced Ca^{2+} Release Mediated by *DMI1*

To test the effect of the Ser/Ala polymorphism in modulating Ca^{2+} signaling, we developed a Ca^{2+} -induced Ca^{2+} release assay in Human Embryonic Kidney cells (HEK-293) expressing the Yellow Cameleon 3.6 (YC3.6) Ca^{2+} indicator (see Supplemental Figure 8A online). In these cells, a *DMI1*:green fluorescent protein (GFP) fusion was localized to the nuclear envelope (see Supplemental Figures 8B and 8C online). Oscillations in the Förster resonance energy transfer/cyan fluorescent protein (FRET/CFP) ratio resulting from YC3.6 are directly proportional to the free Ca^{2+} available in the cytosol. The addition of 2 mM $CaCl_2$ to the external bath solution resulted in a drastic increase in the FRET/CFP ratio in HEK-293

cells expressing *DMI1*. A stepwise increase in the Ca^{2+} concentration of external bath solution from 2 to 10 mM (an increase of 2 mM for every step) resulted in Ca^{2+} transients coupled with periodic oscillations or spikes in the FRET/CFP ratio in HEK-293 cells expressing *DMI1* (Figure 7). Such an upward shift, or oscillations, in the FRET/CFP ratio was not observed in control cells expressing only YC3.6, even at a 10 mM Ca^{2+} concentration (Figure 7). Although some control cells shrank in response to a high concentration of $CaCl_2$ in the external solution, they never displayed any increase in the FRET/CFP ratio or spikes, even at 10 mM $CaCl_2$ (Figure 7). These results demonstrate that *DMI1* has the ability to activate Ca^{2+} channels, thereby modulating a Ca^{2+} -induced Ca^{2+} release in animal HEK-293 cells. These Ca^{2+} oscillations seem to originate from internal Ca^{2+} stores, since the application of 10 mM cadmium did not inhibit the spiking pattern initiated by the prior addition of Ca^{2+} to the external bath (see Supplemental Figure 8D online). The spiking continued even 10 min after the application of cadmium to the external bath (see Supplemental Figure 8D online). However, application of cadmium before the Ca^{2+} treatment totally prevented the elicitation of spikes, probably due to the inactivation of Ca^{2+} channels responsible for the induction of Ca^{2+} transients (see Supplemental Figure 8E online).

HEK-293 cells expressing the modified *dmi1* mutant allele *dmi1(A294S)*, which mimics the filter of *Lj-CASTOR/POLLUX*, were unable to induce Ca^{2+} -induced Ca^{2+} transients and spikes at 2 and 4 mM Ca^{2+} (Figure 7). However,

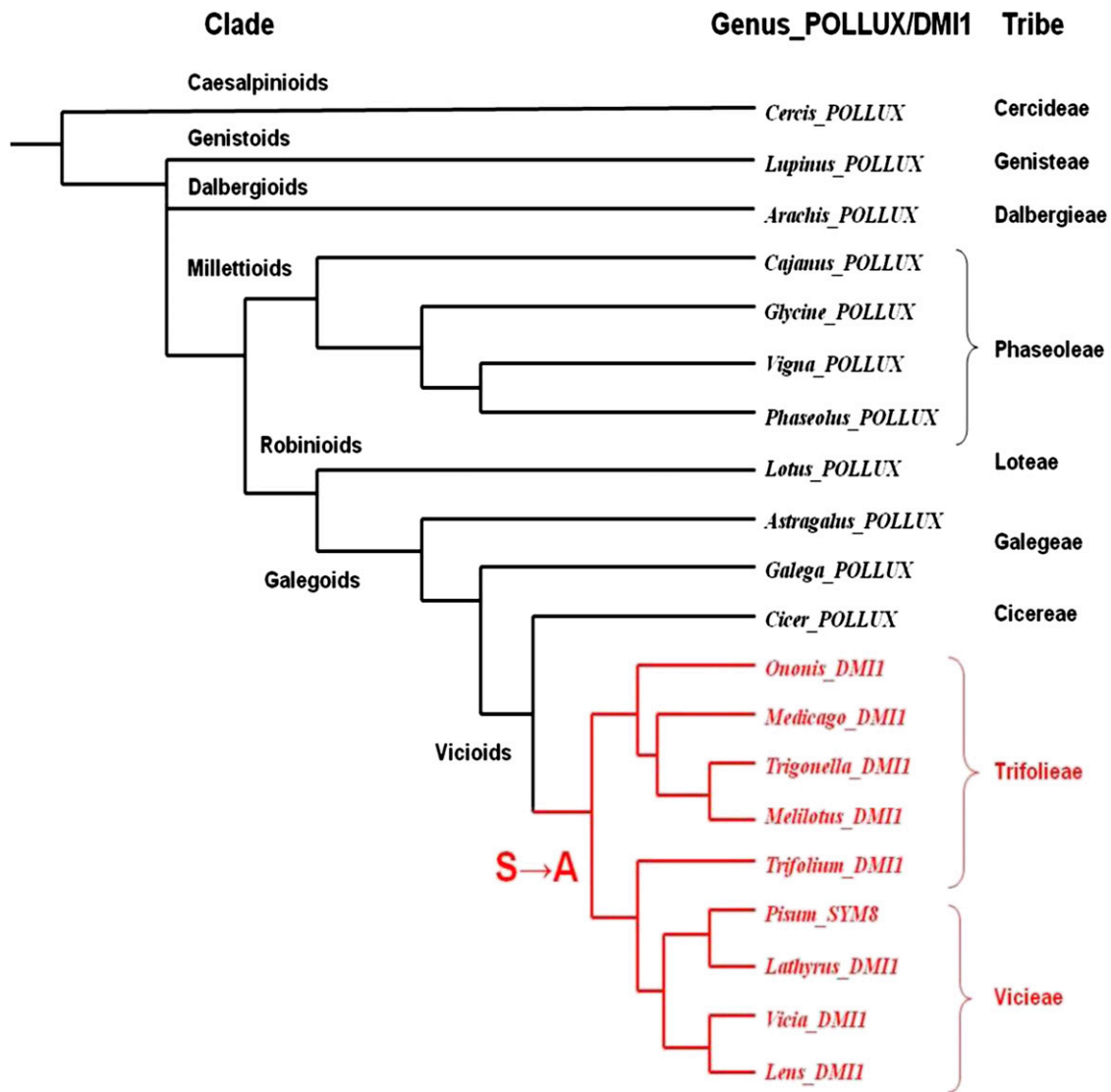


Figure 4. Distribution of Lj-POLLUX (-ADSGNHA-) and DMI1 (-ADAGNHA-) Homologs in Legume Phylogeny.

The possible position of occurrence of the Ser-to-Ala substitution is indicated by an arrow in the phylogenetic tree. The members represented in black have ADSGNHA as selectivity filter, and the members represented in red (Trifolieae and Viciae tribes) have ADAGNHA as selectivity filter. Legume phylogeny was reconstructed based on a previous report (Wojciechowski et al., 2004).

these cells displayed Ca^{2+} transients and a few spikes when the Ca^{2+} concentration in the external bath reached 6 and 10 mM (Figure 7). Ca^{2+} -induced Ca^{2+} transients were absent in cells expressing *dmi1(A294V)*, which mimics a null mutant of pea *SYM8* (Edwards et al., 2007). Similarly, cells expressing an empty vector control did not elicit any Ca^{2+} transient either (Figure 7). These results confirmed that the efficiency of DMI1 in mediating Ca^{2+} spiking in HEK-293 cells is defined by the Ala residue in the filter region.

DISCUSSION

In this study, we functionally characterized *M. truncatula* CASTOR and DMI1 and their *L. japonicus* homologs, CASTOR and

POLLUX. The cation channels DMI1, Lj-POLLUX, and Lj-CASTOR are required for Nod factor-induced Ca^{2+} spiking. They probably act either as counter-ion channels to compensate for the positive charge release from the Ca^{2+} store during each spiking event or activate Ca^{2+} channels by changing the membrane potential of nuclear membranes (Charpentier et al., 2008; Matzke et al., 2009). Our data indicate that these ion channels have different functional properties in symbiotic signaling. In our rescue assays, Lj-CASTOR and Lj-POLLUX together were required to rescue *dmi1*. By contrast, DMI1 and SYM8 alone were sufficient to rescue an Lj-castor pollux double mutant, indicating an improved ability of DMI1 and SYM8 over Lj-CASTOR and Lj-POLLUX. Unlike DMI1 and SYM8, Lj-POLLUX failed to rescue the symbiotic defects of Lj-castor, Lj-castor pollux, and *dmi1* in our study.

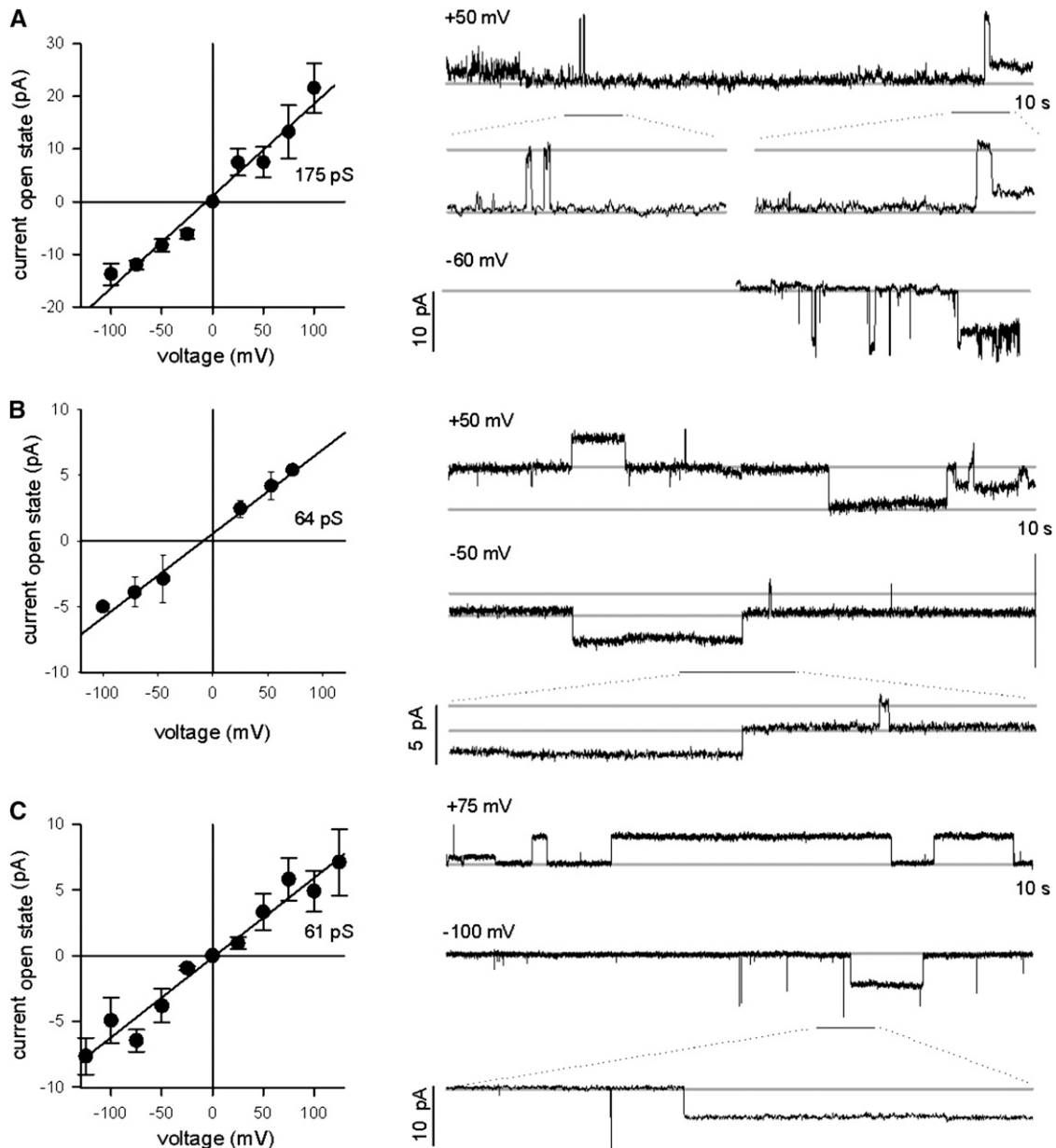


Figure 5. Conductance of Lj-CASTOR, DMI1, and Lj-CASTOR^{S266A} in the Presence of Potassium Chloride.

Conductance of Lj-CASTOR (**A**), DMI1 (**B**), and Lj-CASTOR^{S266A} (**C**) is based on single-channel open-close events at different voltages, as shown in the traces at the right side of each panel. Conductance in picosiemens was calculated as the ratio between the difference of current (I) measured in the open and closed state and the voltage (V) applied [conductance_(pS) = $I_{(pA)}/V_{(mV)}$]. In the presence of KCl, Lj-CASTOR has a significantly higher conductance than DMI1 and Lj-CASTOR^{S266A}. These two channels have a similar intermediate conductance.

This observation differs from a previous report where Lj-POLLUX was shown to rescue Lj-castor (Charpentier et al., 2008). That may be due to different experimental conditions and Lj-castor alleles used. In the previous study, a single Lj-castor allele with a nonsense mutation (W93*) was used (Charpentier et al., 2008), whereas, in this work, we used three different Lj-castor alleles, including two null mutants (Lj-castor-8 and G00532-21), both of which completely lacked the genomic region. None of the

three mutant lines tested in this study were fully rescued for nodulation by Lj-POLLUX (Table 1).

In this study, nodules were categorized into functional nodules and bumps in both *M. truncatula* and *L. japonicus* experiments (Tables 1 and 2). The partial rescue phenotypes (presence of nodule bumps) observed in Lj-castor and Lj-castor pollux mutants rescued by Lj-POLLUX were similar to those observed in Lj-pollux and Lj-castor pollux mutants rescued by Lj-CASTOR.

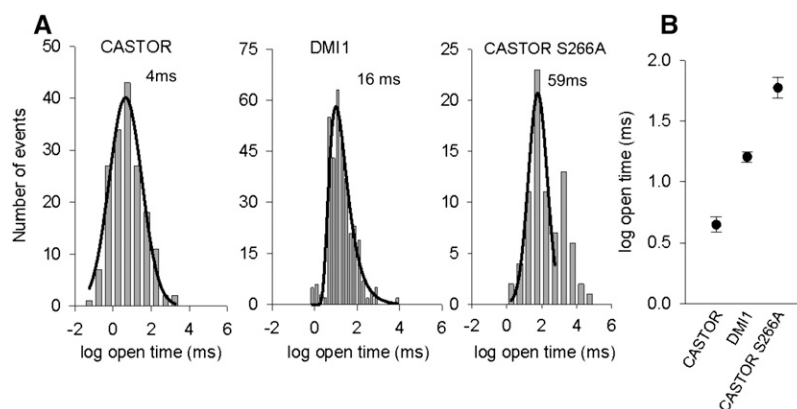


Figure 6. Increase in the Mean Open Time of DMI1 and Lj-CASTOR^{S266A} versus Lj-CASTOR.

(A) Open-time duration histograms obtained in symmetrical 250 mM KCl, at various voltages, for Lj-CASTOR, DMI1, and Lj-CASTOR^{S266A}. Graphs have a logarithmic scale on the x axis. Histograms were best fitted with a Gaussian curve for Lj-CASTOR and Lj-CASTOR^{S266A} and logarithmic curve for DMI1. Mean open times were obtained by pooling single channel currents from three trials with two different protein batches for Lj-CASTOR, two trials with one protein batch for DMI1, and four trials with three protein batches for Lj-CASTOR^{S266A}.

(B) Mean open time values for Lj-CASTOR (4 ± 1 ms), DMI1 (16 ± 1 ms), and Lj-CASTOR^{S266A} (59 ± 1 ms), with respective SE from the Gaussian fit for Lj-CASTOR and Lj-CASTOR^{S266A} and logarithmic for DMI1. Histograms and fitting were done with SigmaPlot.

With the availability of several mutants for rescue assays, we demonstrated that not only Lj-CASTOR, but also Lj-POLLUX, lacks the integrated role of DMI1 and SYM8. These observations are further supported by the inability of rice *POLLUX* to rescue *dmi1* when expressed alone, in which only bumps devoid of bacteria were observed (Chen et al., 2009). By contrast, pea *SYM8* could rescue not only *dmi1* (Edwards et al., 2007), but also Lj-*castor*, Lj-*pollux*, and the Lj-*castor pollux* double mutant of *L. japonicus*, just like DMI1 (this study).

DMI1 and SYM8 have an identical selectivity filter ADAGNHA that is absent from CASTOR and POLLUX of *L. japonicus* and rice. Our data support the current knowledge that specific residues in this region play a key role in the permeation of ion channels. For example, substitutions in the Asp or the Ala residue (ADAGNHA) to Val disrupted the function of SYM8 (Edwards et al., 2007), and substitution in the first Ala residue (ADSGHNA) disrupted CASTOR function in the Lj-*castor-2* mutant (Charpentier et al., 2008).

In this study, a Ser-to-Ala substitution in the filter region of POLLUX (ADSGNHA) conferred a superior ability to this channel and has been retained through natural selection in the *Trifolieae* and *Vicieae* tribes. *POLLUX*^{S329A} gained the ability to rescue the nodulation defects of both *dmi1* and Lj-*castor pollux* mutants. Reciprocally, *DMI1*^{A294S} lost its ability to rescue Lj-*castor*, Lj-*castor pollux*, and *dmi1* in Mt-CASTOR-RNAi roots. Our conclusions have been validated even outside of the legume family using *Arabidopsis* POLLUX.

We propose that the Ser-to-Ala substitution might introduce conformational changes at the selectivity filter. Homology modeling of DMI1 and its homologs identified possible conformational differences at the filter region of these channels due to the Ser/Ala polymorphism (Figures 8A and 8B). The Ala (Ala-294) residue in DMI1 interacts only weakly with the Asp (Asp-293) from the adjacent subunit (Figure 8A). By contrast, the hydroxyl

group of Ser in Lj-CASTOR (Ser-266) and Lj-POLLUX (Ser-329) interacts with the Asp from the adjacent subunit (Asp-265 in Lj-CASTOR and Asp-328 in Lj-POLLUX), restricting the Asp residue in a tight position, in a conformation suitable for conduction (Figure 8B). The Asp is apparently stabilized in a position where one of the two hydroxyl groups on its side chain faces the ion conduction pathway, possibly contributing to divest incoming ions of their hydration shell and thus permitting the higher conductance that is observed in the Lj-CASTOR channel (Figure 5A). At the equivalent position in the MthK and KcsA channels, the hydroxyl from the side chain of the Thr at the cytoplasmic end of the filter (TVGYGD) also divests the potassium ion of its hydration shell (Ye et al., 2010).

As reported previously, Lj-CASTOR displays K⁺ selectivity (Charpentier et al., 2008). In this study, the Ser-to-Ala substitution in the filter region of Lj-CASTOR^{S266A} conferred only a moderate conductance to this channel (61 pS against 175 pS for Lj-CASTOR), similar to DMI1 (64 pS). In this study, we could not test the electrophysiological properties of Lj-POLLUX and Lj-POLLUX^{S329A} directly. In spite of several attempts, Lj-POLLUX could not be produced through in vitro transcription/translations similar to Lj-CASTOR, Lj-CASTOR^{S266A}, and DMI1 and was therefore unavailable for the planar lipid bilayer system. Hence, we relied on Lj-CASTOR, Lj-CASTOR^{S266A}, and DMI1 to test our hypotheses. Although Lj-CASTOR and Lj-POLLUX may show differences in their regulatory mechanisms, they have identical ion selectivity filter regions and likely have similar ion selectivity and conductivity properties. The failure of Lj-CASTOR^{S266A} to rescue Lj-*pollux*, Lj-*castor pollux*, and Lj-*dmi1* mutants may be due to differences in the regulatory mechanism. This hypothesis is supported by the fact that Lj-POLLUX^{S329A} is able to rescue the *dmi1* mutation, while Lj-CASTOR^{S266A} failed to rescue *dmi1* in *M. truncatula*, although Lj-CASTOR^{S266A} is still functional and able to rescue the Lj-*castor* mutation in *L. japonicus*. This

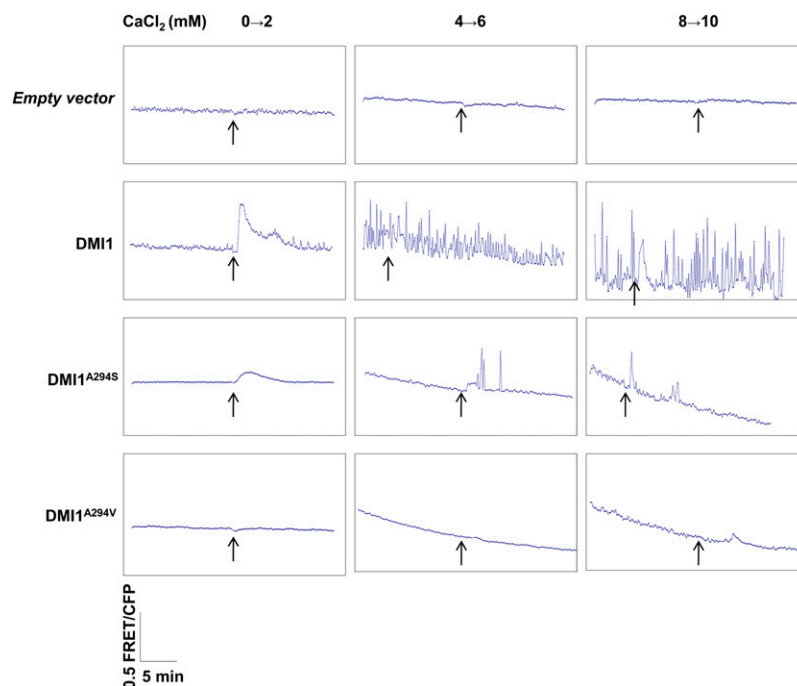


Figure 7. Influence of DMI1 and Modified Alleles on Ca^{2+} -Induced Ca^{2+} Release in HEK-293 Cells.

Vector control-expressing cells did not reflect any change in the FRET/CFP ratio after the addition of 2 to 10 mM CaCl_2 ($n = 10$). DMI1-expressing cells showed Ca^{2+} influx at 2 mM CaCl_2 and periodic oscillations (Ca^{2+} spiking) at higher concentrations of Ca^{2+} (6 and 10 mM) ($n = 10$). The cells expressing the *dmi1*^{A294S} allele were affected in the initial Ca^{2+} influx at 2 mM and showed only a low number of Ca^{2+} spikes at higher concentrations of 6 and 10 mM CaCl_2 ($n = 10$). The cells expressing a nodulation defective mutant allele, *dmi1*^{A294V}, were affected for both Ca^{2+} influx and Ca^{2+} spiking at 2 to 10 mM CaCl_2 , similar to a control empty vector expressing cell ($n = 10$). Arrow indicates the point of application of CaCl_2 to the bath solution. [See online article for color version of this figure.]

explains that Lj-CASTOR, Lj-POLLUX, and DMI1 have distinct states of functionality and that mere conversion to an intermediate ion channel with a long open state in Lj-CASTOR^{S266A} does not rescue *dmi1*, but a similar modification in Lj-POLLUX^{S329A} rescues *dmi1*. We used FRET-based assays as a quantitative measure to ascertain the effect of this Ala-to-Ser substitution on the ability of these channels to mediate intracellular Ca^{2+} oscillations. We showed that the ability of DMI1 to allow Ca^{2+} -induced Ca^{2+} release in HEK-293 cells is drastically affected when Ala was substituted for Ser to mimic the filter region of Lj-CASTOR and Lj-POLLUX. These observations correlate well with the observed superior functionality of DMI1, which integrates the roles of Lj-CASTOR and Lj-POLLUX. We also observed an increase in the mean open time for DMI1 (fourfold) and Lj-CASTOR^{S266A} (15-fold) over wild-type Lj-CASTOR (4 ± 1 ms). These data indicate that the Ala residue in DMI1 has a stabilizing effect on the open state of the channel. Our homology-based modeling predicts that the smaller side chain of the Ala compared with Ser allows a more compact packing against the pore helix behind the filter sequence (ADAGNHA). This would be opposite to the stabilization of the Asp residue by the Ser, which might explain the higher conductance of the filter with the Ser residue (ADSGNHA), as we discussed earlier.

Similarly, point mutations in the pore region of the temperature-activated transient receptor potential cation channel (TRPV1)

alter the gating kinetics and duration of the channel open state. It was shown that wild-type TRPV1 channel displayed both short (<1 ms) and long (~10 ms) open states, while the loss-of-function mutants affected in the pore region only displayed short open states (<1 ms) (Grandl et al., 2010). Together with our study, these observations suggest that the duration and stability of the open state of ion channels determine the channel efficiency.

To our knowledge, there is no report of a naturally occurring mutation in the filter region of an ion channel leading to an improvement of function, as seen in this study. Charpentier et al. (2008) proposed a model in which Lj-CASTOR and Lj-POLLUX act as counter-ion channels that compensate for the positive charge associated with Ca^{2+} release during spiking. This model predicts a significant ion flow through the channels during spiking. This quantitative flux model was also consistent with the idea that two channels (Lj-CASTOR and Lj-POLLUX) are required for calcium spiking. However, the observed conductances of the channels are not simple to reconcile with this model because a higher K^+ conductance of the channels would be expected to improve the counter ion permeation capability. By contrast, we observed that DMI1 shows moderate ion conductance, while the Lj-castor-2 channel with high conductance could not support calcium spiking (Charpentier et al., 2008), implying that ion conductance alone is not the only factor determining the functionality of these channels in the generation of

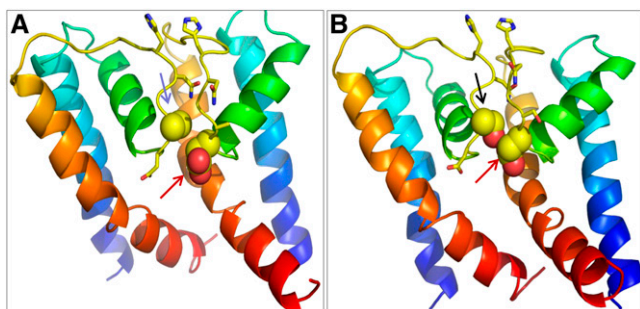


Figure 8. Homology-Based Protein Models Depicting the Structure of the Pore Region, Specifically the Filter Region of DMI1, Lj-CASTOR, and Lj-POLLUX.

Each model shows two monomers of the putatively tetrameric channels. The blue arrow in **(A)** indicates Ala (DMI1^{A294}), the black arrow in **(B)** indicates Ser (Lj-POLLUX^{S329} and Lj-CASTOR^{S266}), and the red arrows in both panels indicate Asp residues (Lj-POLLUX^{D328}, Lj-CASTOR^{D265}, and DMI1^{D293}).

(A) The orientation of Asp is affected by the weak interaction with Ala in DMI1.

(B) The orientation of Asp is affected by the strong interaction with Ser in Lj-POLLUX and Lj-CASTOR.

calcium spiking. It is likely that the duration of the open state and stability of the pore are also important factors regulating the improved functionality of DMI1 over Lj-CASTOR and Lj-POLLUX.

In mammalian cells, action potentials (spikes) have been more thoroughly characterized. Neurons and muscle cells generate action potentials largely by regulating the conductance for Na⁺ and K⁺. Na⁺ carries the inward depolarizing current and K⁺ carries the outward hyperpolarizing current. In some neurons, Ca²⁺ carries the inward current instead of Na⁺. In these cases, the K⁺ channels are involved in setting the threshold for Ca²⁺ spike initiation and in limiting the duration of each spike (Golding et al., 1999). Reference conductance levels for K⁺ channels mediating action potentials in animal cells are, for example, 200 pS for large conductance BK (big potassium) channels (Lancaster and Nicoll, 1987), 10 pS for small conductance SK (small conductance calcium-activated potassium) channels (Köhler et al., 1996), and 30 to 50 pS for intermediate/moderate conductance ROMK (renal outer medullary potassium) channels (Sackin et al., 2005). Thus, during evolution, the Ser-to-Ala substitution in the filter region converted a large conductance channel (Lj-CASTOR and Lj-POLLUX) to a moderate conductance channel (DMI1) with enhanced functionality in symbiosis.

Based on its analogy to the animal action potential (Hodgkin and Huxley, 1952; Barnett and Larkman, 2007), the generation of nuclear Ca²⁺ spiking during symbiotic signaling in host plants is expected to require at least three types of ion channels/pumps: the voltage-sensing Ca²⁺ channel(s), the counter-ion channel(s), and the Ca²⁺ pump(s). *L. japonicus* CASTOR and POLLUX, as well as *M. truncatula* DMI1, are localized to the nuclear envelope (Riely et al., 2007; Charpentier et al., 2008). In a recent study, we demonstrated the role of *M. truncatula* Ca²⁺ ATPase, MCA8, in Nod factor-induced calcium spiking, and we observed

localization of MCA8 to both the inner nuclear membrane (INM) and outer nuclear membrane (ONM), similar to DMI1, suggesting their close proximity on the nuclear membranes and their coordinated role in nuclear calcium spiking (Capoen et al., 2011). Evidence for the presence of Ca²⁺ pumps that could replenish the nuclear envelope lumen of Ca²⁺ ions against their concentration gradient was initially shown in nuclei prepared from carrot (*Daucus carota*) cells. It was also shown that Ca²⁺ could be transported across nuclear membranes in an ATP-dependent manner (Bunney et al., 2000), and immunogold labeling identified a homolog of the sarco(endo)plasmic reticulum Ca²⁺ ATPase (SERCA) pump in the nuclear envelope of tomato (*Solanum lycopersicum*) root cells (Downie et al., 1998).

Nuclear envelope-residing calcium channels mediating calcium spiking have not been reported yet. However, two major types of voltage-gated Ca²⁺ permeable channel activities have been recorded on the plasma membrane by electrophysiological methods. These studies suggest the presence of depolarization-activated Ca²⁺ channels (Thuleau et al., 1994; Thion et al., 1998) and hyperpolarization-activated Ca²⁺ channels on the plasma membrane (Shang et al., 2005; Davies and Walker, 2008), although the genes encoding these Ca²⁺-permeable channels have not been identified. A less specific activation mechanism, such as voltage sensing, is compatible with a more general use of such Ca²⁺ channels in various signaling pathways. Although no experimental data are currently available to support the polarization state of the INM and ONM, studies indicate the existence of a potential across the nuclear envelope that results in the nucleus having a more negative charge than the cytoplasm (Loewenstein and Kanno, 1963). Additionally, a recent study shows periodic oscillations of membrane potential upon release of Ca²⁺ from the nuclear envelope (Yamashita, 2011). Given the lack of experimental values, and since the potential across the plasma membrane is negative toward the cytoplasmic side, it is likely that the INM and ONM are also negatively charged on the cytoplasmic side relative to the perinuclear space.

Model Depicting the Role of DMI1 and the POLLUX and CASTOR Duo during Nod and Myc Factor-Induced Ca²⁺ Spiking

Based on our experiments on the channel activities described above, the solo-sufficiency of DMI1 versus the Lj-CASTOR-POLLUX duo, we propose a speculative model explaining the mechanism of nuclear Ca²⁺ spiking (Figure 9). Yet unidentified symbiotic secondary messengers activate the cation channels (Lj-CASTOR and Lj-POLLUX/DMI1), resulting in the flow of K⁺ ions from the cytoplasm into the perinuclear space. This causes the ONM to become hyperpolarized, and because of its close proximity, the INM also becomes hyperpolarized. When a certain degree of hyperpolarization is achieved, the hyperpolarization-gated Ca²⁺ channels are activated, resulting in Ca²⁺ flow out of the perinuclear space to the cytoplasm and nucleoplasm, which leads to Ca²⁺ spiking. The raise in Ca²⁺ concentration is sensed by cation channels and results in Ca²⁺-mediated blockage or inactivation. Simultaneously, the Ca²⁺ flow across the membranes results in depolarization of the nuclear membranes and then closure of Ca²⁺ channels. The Ca²⁺ is pumped back into

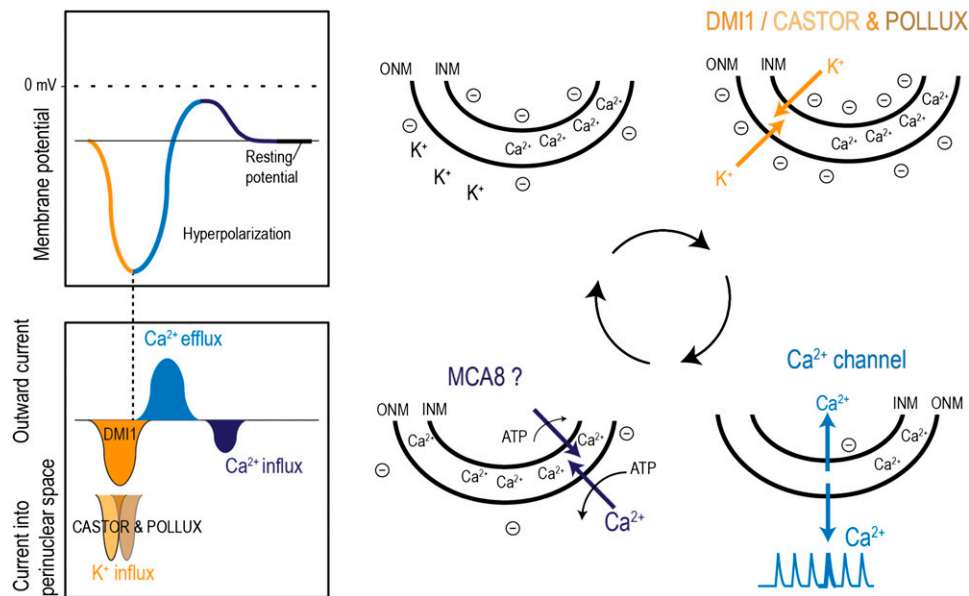


Figure 9. Proposed Model Depicting the Role of DMI1 and the POLLUX and CASTOR Duo during Nod and Myc Factor–Induced Ca^{2+} Spiking.

A yet unknown symbiotic secondary messenger activates cation channels, DMI1 or the CASTOR-POLLUX duo. CASTOR and POLLUX together are required to permeate the K^+ ions in favor of their concentration gradient from the cytoplasm into the perinuclear space. Although these two channels have higher conductance than DMI1, perhaps due to their shorter open lifetime, they are both indispensable to sustain the ion flow and subsequent nuclear membrane hyperpolarization during the minimum amount of time required to activate the Ca^{2+} channel. However, DMI1, with its longer open time, has a larger net flow of K^+ ions and is hence able to hyperpolarize the nuclear membrane without the help of the CASTOR homolog. This causes the ONM to become hyperpolarized, and because of its close proximity, the INM also becomes hyperpolarized. When a certain degree of hyperpolarization is achieved, hyperpolarization-gated Ca^{2+} channels are presumably activated. Ca^{2+} flows out of the perinuclear space to the cytoplasm and nucleoplasm, giving rise to a Ca^{2+} spike. The cation channels, upon sensing the Ca^{2+} , are blocked or inactivated. Simultaneously, the Ca^{2+} flow reduces the hyperpolarization of the nuclear membranes, resulting in the closure of hyperpolarization-gated Ca^{2+} channels. Finally, the Ca^{2+} ions are pumped back into the perinuclear space (the calcium store), by the Ca^{2+} ATPase, MCA8, bringing the membrane back to its resting potential, ready to reinitiate the cycle.

the perinuclear space (calcium store) by Ca^{2+} ATPases such as MCA8.

This model explains the apparent synchronization of the Ca^{2+} release channels across the nuclear envelope. The Ca^{2+} release channels must be activated and open simultaneously to generate a rapid spike. A change in the membrane potential is therefore a more likely trigger than the activation of these channels (one by one) by diffusible symbiotic secondary messengers. According to the proposed model, it is possible that an intermediate conductance channel, such as DMI1, may be able to outperform two large conductance channels, such as Lj-CASTOR and Lj-POLLUX, through its longer open periods and thus facilitate a bigger net flow of K^+ ions (Figure 6). Considering that the measured conductance of Lj-CASTOR is approximately threefold higher than that of DMI1, the fourfold reduction of Lj-CASTOR open time may not be sufficient to explain the integrated role of DMI1 versus the Lj-CASTOR/POLLUX duo. Maybe Lj-CASTOR and Lj-POLLUX have to work together, opening one after the other and therefore creating the change in membrane potential for a certain minimal time period required by activation of the voltage-gated Ca^{2+} channel.

Finally, from the model described, the justification for the different functionality of CASTOR and POLLUX in the complementation experiments can be partly attributed to a possible

offset in activation time required for each channel, to different affinities to Ca^{2+} as a potential blocker agent or maybe just to the different distribution of the two channels in the nuclear envelope.

Evolution involves the selection of beneficial alleles through improved fitness of the carrier. However, only few examples are documented in which the selective advantage of a novel allele is so well characterized at the mechanistic level. Based on the electrophysiological studies and cross-species rescue assays, we propose that a functional improvement of a symbiotic ion channel DMI1 was facilitated by a single amino acid substitution within the selectivity filter region. This substitution was responsible for the conversion of a large conductance channel with a short open state into an intermediate conductance channel with likely a longer open lifetime, which is associated with the capacity of DMI1 to act as a more efficient counter ion channel during Ca^{2+} signaling, and explains why this Ala residue has been positively selected and maintained in the Viciae and Trifolieae clades.

METHODS

Plant Material

RNAi and rescue assays in *Medicago truncatula* were performed in wild-type Jemalong A17 and the *dmi1-4* mutant line (GY15-3F-4), respectively.

Rescue assays in *Lotus japonicus* were performed on Lj-*castor* mutants (Lj-*castor-4*, Lj-*castor-8*, and G00532-21), the Lj-*pollux* mutant (*pollux-2*), and the Lj-*castor pollux* double mutant. Lj-*castor-8* and G00532-21 completely lack the genomic region of Lj-CASTOR. The Lj-*castor pollux* double mutant was identified among F2 progeny from a cross between Lj-*castor-5* and Lj-*pollux-2* mutants. A complete list of all the *M. truncatula* and *L. japonicus* mutant lines used in this study with the information on the nature of the mutation is provided in Supplemental Table 1 and Supplemental References 1 online.

Mt-CASTOR Coding Sequence

The full-length coding sequence of Mt-CASTOR was obtained by a combination of RT-PCR and 3' rapid amplification of cDNA ends (RACE). RNA ligase-mediated RACE was performed using GeneRacer (Invitrogen). The nested primers P₁, P₂, and P₃ used to perform 3' RACE were designed based on Mt-CASTOR ESTs available on the *M. truncatula* genome project online database. Since the EST sequences obtained from the public database already contained the beginning of the gene, 5' RACE-PCR was not performed. The full-length product was amplified using the primer set P₄ and P₅ and cloned into the entry vector pENTR/D-TOPO (Invitrogen) for further use. A list of all the primers used in this study is provided in Supplemental Table 2 online.

RNAi of Mt-CASTOR and DMI1

A 451-bp fragment at the 5' coding region of Mt-CASTOR was amplified using the primers P₆ and P₇ and cloned into a modified hairpin RNAi-expressing binary vector, pK7GWIWG2(II)-R, containing the constitutively expressed fluorescent marker *DsRED1* (Riely et al., 2011). As a positive control, we performed RNAi-based gene knockdown of *DMI1*. Primers P₈ and P₉ were used to amplify a 413-bp fragment of *DMI1*, which was cloned into pK7GWIWG2(II)-R. Empty vector was used as the negative control. *Agrobacterium rhizogenes*-mediated root transformation was performed to deliver the constructs into Jemalong A17 as previously described (Boisson-Dernier et al., 2001). Reduction in the Mt-CASTOR expression level was confirmed by RT-PCR using the primers P₁₀ and P₁₁, and Mt-*ACTIN* expression was measured using primers P₁₂ and P₁₃. Nodulation and AM assays were performed as previously described (Limpens et al., 2004; Javot et al., 2007). A total of 90 transiently transgenic plants underwent the nodulation assay for each construct. From three biological replications, a total of 36 plants were subjected to the mycorrhization assay with the Mt-CASTOR-RNAi construct and 24 plants with the empty vector control. For the AM assay, *Glomus intraradices* (IRBV'95 Mycorise ASP; Premier Tech Biotechnologies) spore suspension was used. Both Mt-CASTOR-RNAi-expressing transgenic roots and control roots were sampled for analysis of Mt-*PT4* expression using the primers P₁₄ and P₁₅.

cDNA Synthesis and RT-PCR

Total RNA was isolated using an RNeasy Plant Mini Kit (Qiagen) and subjected to rDNase enzyme (DNA-free; Ambion) to remove residual genomic DNA contamination. From each sample, 1 µg total RNA was used for cDNA synthesis using the SuperScript III first-strand synthesis kit (Invitrogen). An equal amount of cDNA was used as template for RT-PCR to measure the expression level of candidate genes. Mt-*Actin* was used as a reference gene for loading control.

Cross-Species Rescue Assays in *M. truncatula* and *L. japonicus*

Lj-CASTOR and Lj-POLLUX were expressed in the *dmi1-4* mutant of *M. truncatula*. For constitutive expression of full-length proteins under the

control of 35S_{pro}, Lj-CASTOR was cloned into the binary vector pK7WG2D, which has GFP as a visible marker. Lj-POLLUX was cloned into the modified binary vector pK7FWG2-R, which carries *DsRED1* as a visible marker. To drive the expression of Lj-CASTOR and Lj-POLLUX under their respective native promoters (2300 and 2800 bp, respectively), the constructs pK7RWG2:Lj-CASTOR_{pro}:Lj-CASTOR and pK7RWG2:Lj-POLLUX_{pro}:Lj-POLLUX were used. To express Lj-CASTOR and Lj-POLLUX under the influence of the *DMI1* promoter (1500 bp), the 35S_{pro} in pK7FWG2-R was replaced with the promoter of *DMI1*. The binary vector pUB-GW-GFP was used to express Lj-CASTOR and Lj-POLLUX under the influence of the Lj-*Ubiquitin1* promoter (Maekawa et al., 2008). At-POLLUX was cloned into pK7WG2D for rescue assays in *dmi1-4*. *DMI1*, *DMI1*^{A294A}, *SYM8*, and Mt-CASTOR constructs were introduced into the *L. japonicus* mutants by root transformation with *A. rhizogenes* LBA1334, as previously described (Banba et al., 2008). Nodulation and arbuscular mycorrhization assays in *L. japonicus* were performed as previously described (Banba et al., 2008).

Site-Directed Mutagenesis

Modification of the filter region of Lj-POLLUX and Lj-CASTOR was achieved by point mutations in Lj-POLLUX (T985G) and Lj-CASTOR (T976G), both of which mimic the filter region of *DMI1* at the amino acid level. The point mutation G880T in *DMI1* was performed to mimic the filter region of Lj-CASTOR/Lj-POLLUX at the amino acid level. To mimic the filter region of *DMI1* in At-POLLUX point mutations, T709G and G716A were introduced. The QuickChange site-directed mutagenesis kit (Stratagene) was used to perform point mutations on the entry clones pENTR/D:Lj-CASTOR, pDONR221:Lj-POLLUX, pDONR221:*DMI1*, and pENTR1A:At-POLLUX. Primers used for site-directed mutagenesis were as follows: The primer sets P₁₆-P₁₇, P₁₈-P₁₉, P₂₀-P₂₁, P₂₂-P₂₃, and P₂₄-P₂₅ were used to generate *DMI1*^{A294S}, Lj-POLLUX^{S329A}, Lj-CASTOR^{S266A}, At-POLLUX^{S237A}, and At-POLLUX^{S237A S239N}, respectively. These mutants were cloned into the Gateway binary vector pK7WG2D by LR recombination (Invitrogen) for rescue assays in *M. truncatula* and *L. japonicus*.

Phylogenetic Analyses

A total of 309 bp of nucleotide sequences flanking the filter region of *DMI1* homologs was amplified from genomic DNA of legume genera, such as *Cercis*, *Lupinus*, *Arachis*, *Cajanus*, *Glycine*, *Vigna*, *Phaseolus*, *Astragalus*, *Galega*, *Cicer*, *Ononis*, *Medicago*, *Trigonella*, *Melilotus*, *Trifolium*, *Pisum*, *Lathyrus*, *Vicia*, and *Lens*, using the primers P₂₆ and P₂₇. The PCR product sequences were aligned using the multiple alignment program T-Coffee (Notredame et al., 2000), and alignment curation was performed using Gblocks (Castresana, 2000). The coding sequence of *DMI1* was used as a reference for translation of nucleotide sequences to amino acid sequences at the pore region. Homologs across legume genera were grouped into *DMI1* and POLLUX type, based on amino acid sequence in the filter region, ADAGNHA/ADSGNHA. The amino acid sequence alignment of the pore region of all the legume genera is presented in Supplemental Data Set 1 online. Since the sequence length of the pore region obtained from different legume species was too short (309 bp) for phylogenetic analyses with a high confidence level, a legume phylogeny with selected legume genera was reconstructed based on the existing phylogenetic tree (Wojciechowski et al., 2004).

Homology Modeling

The MthK pore region was used as a model for the tetrameric pore region. The amino acid sequences of *DMI1*, Lj-CASTOR, Lj-POLLUX, Mt-CASTOR,

DMI1^{A294S}, Lj-POLLUX^{S329A}, and Lj-CASTOR^{S266A} were aligned to MthK using the alignment program MUSCLE (<http://www.ebi.ac.uk/Tools/muscle/index.html>) (see Supplemental Figure 9 online). Then, the pore region of MthK was mutated to the one of candidate proteins in the molecular modeling program SYBYL (Tripos). The alignment was further adjusted by visualizing the mutated filter region for reasonable fits of the side chains. A conserved Gly in the filter region was used to position the remaining amino acids in the alignment. No gaps or insertions were made and the sequences were threaded on the MthK structure. A similar approach was used to model the filter region of DMI1 homologs. SYBYL was then used to energy minimize the models for convergence using the Tripos force field and Gasteiger-Huckel charges in the models. Figures of protein models were made with PymOL (<http://www.pymol.org>).

In Vitro Expression and Purification of Lj-CASTOR and DMI1

Lj-CASTOR and Lj-CASTOR^{S266A} were expressed through coupled in vitro transcription/translation and purified as described (Charpentier et al., 2008), with further purification of the hexahistidine-tagged proteins by affinity chromatography on nickel-nitrilotriacetic beads. DMI1 was expressed using a wheat germ in vitro transcription/translation system (5 Prime), and the soluble protein was purified via its hexahistidine tag by affinity chromatography on cobalt TALON resin (Clontech).

Reconstitution in Proteoliposomes and Planar Lipid Bilayer Measurements

Two different setups were used for single channel recordings. First, the channels Lj-CASTOR and Lj-CASTOR^{S266A} were reconstituted in proteoliposomes and measured in a setup previously described (Charpentier et al., 2008). The conductance was recorded at different voltages in symmetrical conditions (250/250 mM KCl). The linear regression of the data points for each voltage was used to define the conductance. All solutions were buffered with 10 mM MOPS/Tris at pH 7.0 or 10 mM HEPES at pH 7.0.

Second, the conductance of the DMI1 channel and the two channels already measured with the first setup were also recorded on bilayers spanning a single micron-sized hole in a glass substrate. This second setup is the automated patch-clamp system Port-a-Patch (Nanion Technologies). The proteins were reconstituted in giant unilamellar vesicles of the lipid 1,2-diphytanoyl-*sn*-glycero-3-phosphatidylcholine (Avanti Polar Lipids), and conductance was measured in symmetrical potassium chloride solution (250 mM) buffered with 10 mM HEPES at pH 7.0. Single channel electrical recordings were performed with an EPC10 USB patch clamp amplifier (Heka Electronics) using the Patchmaster software (Heka Electronics). Data were plotted using SigmaPlot software.

Ca²⁺ Imaging Using YC3.6 and Data Analyses

HEK-293 cells were cultured and transfected as described (Johannessen et al., 2009). Thirty-six hours after transfection, HEK-293 cells expressing DMI1 or modified alleles *dmi1*(A294S) or *dmi1*(A294V) were chosen for confocal microscopy. The complete growth medium in the chamber was replaced with 1 mL of external bath solution (130 mM NaCl, 3 mM KCl, 0.6 mM MgCl₂, 10 mM Glc, and 10 mM HEPES, pH 7.4). Transfected cells with bright YC3.6 expression levels were chosen for FRET analyses (see Supplemental Figure 8A online). The CFP emission (473 to 505 nm) and FRET emission (536 to 546 nm) were collected using a 458-nm primary dichroic mirror and the Meta detector of a Zeiss LSM 510 microscope. Known quantities of CaCl₂ (2 to 10 mM) were applied to the external solution at the 125th cycle. A stepwise increase of 0→2 mM, 2→4 mM, 4→6 mM, 6→8 mM, and 8→10 mM CaCl₂ was required to observe

DMI1-modulated Ca²⁺-induced Ca²⁺ release in HEK-293 cells. We also attempted to trigger Ca²⁺-induced Ca²⁺ release in HEK-293 cells expressing DMI1 by adding 0→2 mM, 0→4 mM, 0→6 mM, 0→8 mM, and 0→10 mM CaCl₂. The addition of CaCl₂ at such high concentrations to steady state HEK-293 cells resulted in a mere transient increase in CaCl₂ concentration and cell bursting in several instances. Hence, a stepwise increase in Ca²⁺ concentration was attempted. The objective fields were scanned once every 7.5 s for a total of 250 cycles. Image analyses were performed using LSM Image Browser version 4.2 (Carl Zeiss). A total of 10 cells were observed for all the constructs at all extracellular CaCl₂ concentrations tested (2 to 10 mM). Background CFP and FRET signal were subtracted from the signals obtained from test cells. The FRET/CFP ratio was calculated for each time point and plotted in the y axis in a scatter diagram over time (min) in the x axis.

Accession Numbers

Primers used for 3' RACE to obtain coding sequence of Mt-CASTOR were designed based on ESTs available at GenBank under accession number CX525932. The coding sequences of DMI1, Mt-CASTOR, Lj-CASTOR, Lj-POLLUX, Ps-SYM8, and At-POLLUX (At5g49960) can be obtained from GenBank with accession numbers XM-003592883, FJ974130, AB162157, AB162158, EF447277, and NM-124375, respectively.

Supplemental Data

The following materials are available in the online version of this article.

Supplemental Figure 1. Sequences and Domain Structures of Mt-CASTOR.

Supplemental Figure 2. RT-PCR Analyses to Validate Mt-CASTOR Gene Silencing, Expression of Mt-PT4, and Coexpression of Lj-CASTOR and Lj-POLLUX in *dmi1*.

Supplemental Figure 3. Rescue of *L. japonicus castor*, *pollux*, and *castor pollux* Double Mutants by Mt-CASTOR, Lj-CASTOR, Lj-POLLUX, DMI1, and SYM8.

Supplemental Figure 4. Rescue of the AM Phenotype in the *L. japonicus castor pollux* Double Mutant and *M. truncatula dmi1* Mutant.

Supplemental Figure 5. Characterization of Nodules and Nodule Bumps Formed in *dmi1* by Rescue Assays with Lj-POLLUX and DMI1 for the Infection Phenotype Using the X-Gal Assay.

Supplemental Figure 6. Characterization of Nodules Formed in the Rescue Assays for Rhizobial Infection Using *hema_{pro}:lacZ* Expression and Nitrogen Fixation Using *nifH_{pro}:uidA* Expression.

Supplemental Figure 7. Traces at Constant Voltage for Lj-CASTOR, Lj-CASTOR^{S266A}, and DMI1.

Supplemental Figure 8. Subcellular Localization of DMI1 in HEK-293 Cells and Investigating the Source of Calcium-Induced Calcium Release.

Supplemental Figure 9. Sequence Alignment of DMI1 Homologs with MthK at the Pore Region.

Supplemental Table 1. List of Lj-CASTOR, Lj-POLLUX, and DMI1 Mutant Alleles Used in This Study.

Supplemental Table 2. List of Primers Used in This Study.

Supplemental References 1. References for the Supplemental Data.

Supplemental Data Set 1. Sequence Alignment of the DMI1 or POLLUX Pore Region of 20 Different Legume Species Generated

Using the Sequence Alignment Program T-Coffee (Notredame et al., 2000).

ACKNOWLEDGMENTS

We thank Jeanne Harris for providing the *Sinorhizobium meliloti* strain *nifH_{pro::uidA}*, Douglas R. Cook for providing genomic DNA of various legumes, Eric Vincill and Edgar Spalding for providing the pIRES2-YC3.6 construct, and Yosuke Umehara for providing G00532-21 seeds. We thank the North Central Regional Plant Introduction Station, USDA, and Washington State University Regional Plant Introduction Station, USDA, for providing seeds of various legumes. We thank Meyer Jackson and Molly Johannessen for providing lab space and technical help with HEK-293 cell culture. We thank Michael R. Sussman for technical guidance and critical reading of the article. We acknowledge the technical support received from Maxime Magne, Ronald Crandall, Guesline Cadet, Gregory Laffen, Derek Nedveck, Adam B. Levin, and Colby Cantu. This research was supported by USDA Hatch WIS01163 and National Science Foundation 0701846 to J.-M.A. and by the Program of Basic Research Activities of Innovative Biosciences (to H.I.-A.). A.C. and M.P. were funded by a grant (PA 493/9-1) from the German research foundation Deutsche Forschungsgemeinschaft to M.P. Confocal microscopy was performed at the University of Wisconsin–Madison Plant Imaging Center and was supported by the National Science Foundation.

AUTHOR CONTRIBUTIONS

J.-M.A., H.I.-A., M.P., E.S., and M.V. designed the research. M.V., A.C., L.H., M.B., and K.A.S. performed the research. M.V., A.C., and L.H. analyzed the data. M.V., J.-M.A., A.C., H.I.-A., and M.P. wrote the article.

Received March 20, 2012; revised May 9, 2012; accepted May 26, 2012; published June 15, 2012.

REFERENCES

- Akiyama, K., Matsuzaka, K., and Hayashi, H.** (2005). Plant-fungal associations: Cue for the branching connection. *Nature* **435**: 750–751.
- Ané, J.M. et al.** (2004). *Medicago truncatula* *DMI1* required for bacterial and fungal symbioses in legumes. *Science* **303**: 1364–1367.
- Ané, J.M. et al.** (2002). Genetic and cytogenetic mapping of *DMI1*, *DMI2*, and *DMI3* genes of *Medicago truncatula* involved in Nod factor transduction, nodulation, and mycorrhization. *Mol. Plant Microbe Interact.* **15**: 1108–1118.
- Banba, M., Gutjahr, C., Miyao, A., Hirochika, H., Paszkowski, U., Kouchi, H., and Imaizumi-Anraku, H.** (2008). Divergence of evolutionary ways among common *sym* genes: *CASTOR* and *CCaMK* show functional conservation between two symbiosis systems and constitute the root of a common signaling pathway. *Plant Cell Physiol.* **49**: 1659–1671.
- Barnett, M.W., and Larkman, P.M.** (2007). The action potential. *Pract. Neurol.* **7**: 192–197.
- Boisson-Dernier, A., Chabaud, M., Garcia, F., Bécard, G., Rosenberg, C., and Barker, D.G.** (2001). *Agrobacterium rhizogenes*-transformed roots of *Medicago truncatula* for the study of nitrogen-fixing and endomycorrhizal symbiotic associations. *Mol. Plant Microbe Interact.* **14**: 695–700.
- Bright, L.J., Liang, Y., Mitchell, D.M., and Harris, J.M.** (2005). The *LATD* gene of *Medicago truncatula* is required for both nodule and root development. *Mol. Plant Microbe Interact.* **18**: 521–532.
- Bunney, T.D., Shaw, P.J., Watkins, P.A., Taylor, J.P., Beven, A.F., Wells, B., Calder, G.M., and Dröbak, B.K.** (2000). ATP-dependent regulation of nuclear Ca^{2+} levels in plant cells. *FEBS Lett.* **476**: 145–149.
- Capoen, W., Sun, J., Wysham, D., Otegui, M.S., Venkateshwaran, M., Hirsch, S., Miwa, H., Downie, J.A., Morris, R.J., Ané, J.M., and Oldroyd, G.E.** (2011). Nuclear membranes control symbiotic calcium signaling of legumes. *Proc. Natl. Acad. Sci. USA* **108**: 14348–14353.
- Castresana, J.** (2000). Selection of conserved blocks from multiple alignments for their use in phylogenetic analysis. *Mol. Biol. Evol.* **17**: 540–552.
- Chabaud, M., Genre, A., Sieberer, B.J., Faccio, A., Fournier, J., Novero, M., Barker, D.G., and Bonfante, P.** (2011). Arbuscular mycorrhizal hyphopodia and germinated spore exudates trigger Ca^{2+} spiking in the legume and nonlegume root epidermis. *New Phytol.* **189**: 347–355.
- Charpentier, M., Bredemeier, R., Wanner, G., Takeda, N., Schleiff, E., and Parniske, M.** (2008). *Lotus japonicus* *CASTOR* and *POLLUX* are ion channels essential for perinuclear calcium spiking in legume root endosymbiosis. *Plant Cell* **20**: 3467–3479.
- Chen, C., Fan, C., Gao, M., and Zhu, H.** (2009). Antiquity and function of *CASTOR* and *POLLUX*, the twin ion channel-encoding genes key to the evolution of root symbioses in plants. *Plant Physiol.* **149**: 306–317.
- Davies, B.W., and Walker, G.C.** (2008). A highly conserved protein of unknown function is required by *Sinorhizobium meliloti* for symbiosis and environmental stress protection. *J. Bacteriol.* **190**: 1118–1123.
- Dénarié, J., Debellé, F., and Promé, J.C.** (1996). Rhizobium lipochitooligosaccharide nodulation factors: Signaling molecules mediating recognition and morphogenesis. *Annu. Rev. Biochem.* **65**: 503–535.
- Downie, L., Priddle, J., Hawes, C., and Evans, D.E.** (1998). A calcium pump at the higher plant nuclear envelope? *FEBS Lett.* **429**: 44–48.
- Edwards, A., Heckmann, A.B., Yousafzai, F., Duc, G., and Downie, J.A.** (2007). Structural implications of mutations in the pea *SYM8* symbiosis gene, the *DMI1* ortholog, encoding a predicted ion channel. *Mol. Plant Microbe Interact.* **20**: 1183–1191.
- Ehrhardt, D.W., Wais, R., and Long, S.R.** (1996). Calcium spiking in plant root hairs responding to Rhizobium nodulation signals. *Cell* **85**: 673–681.
- Golding, N.L., Jung, H.Y., Mickus, T., and Spruston, N.** (1999). Dendritic calcium spike initiation and repolarization are controlled by distinct potassium channel subtypes in CA1 pyramidal neurons. *J. Neurosci.* **19**: 8789–8798.
- Grandl, J., Kim, S.E., Uzzell, V., Bursulaya, B., Petrus, M., Bandell, M., and Patapoutian, A.** (2010). Temperature-induced opening of TRPV1 ion channel is stabilized by the pore domain. *Nat. Neurosci.* **13**: 708–714.
- Groth, M., Takeda, N., Perry, J., Uchida, H., Dräxl, S., Brachmann, A., Sato, S., Tabata, S., Kawaguchi, M., Wang, T.L., and Parniske, M.** (2010). *NENA*, a *Lotus japonicus* homolog of *Sec13*, is required for rhizodermal infection by arbuscular mycorrhiza fungi and rhizobia but dispensable for cortical endosymbiotic development. *Plant Cell* **22**: 2509–2526.
- Gutjahr, C., Banba, M., Croset, V., An, K., Miyao, A., An, G., Hirochika, H., Imaizumi-Anraku, H., and Paszkowski, U.** (2008).

- Arbuscular mycorrhiza-specific signaling in rice transcends the common symbiosis signaling pathway. *Plant Cell* **20**: 2989–3005.
- Harrison, M.J., Dewbre, G.R., and Liu, J.** (2002). A phosphate transporter from *Medicago truncatula* involved in the acquisition of phosphate released by arbuscular mycorrhizal fungi. *Plant Cell* **14**: 2413–2429.
- Hodgkin, A.L., and Huxley, A.F.** (1952). A quantitative description of membrane current and its application to conduction and excitation in nerve. *J. Physiol.* **117**: 500–544.
- Imaizumi-Anraku, H. et al.** (2005). Plastid proteins crucial for symbiotic fungal and bacterial entry into plant roots. *Nature* **433**: 527–531.
- Javot, H., Penmetza, R.V., Terzaghi, N., Cook, D.R., and Harrison, M.J.** (2007). A *Medicago truncatula* phosphate transporter indispensable for the arbuscular mycorrhizal symbiosis. *Proc. Natl. Acad. Sci. USA* **104**: 1720–1725.
- Johannessen, M., Ramachandran, S., Riemer, L., Ramos-Serrano, A., Ruoho, A.E., and Jackson, M.B.** (2009). Voltage-gated sodium channel modulation by sigma-receptors in cardiac myocytes and heterologous systems. *Am. J. Physiol. Cell Physiol.* **296**: C1049–C1057.
- Kistner, C., Winzer, T., Pitzschke, A., Mulder, L., Sato, S., Kaneko, T., Tabata, S., Sandal, N., Stougaard, J., Webb, K.J., Szczyglowski, K., and Parniske, M.** (2005). Seven *Lotus japonicus* genes required for transcriptional reprogramming of the root during fungal and bacterial symbiosis. *Plant Cell* **17**: 2217–2229.
- Köhler, M., Hirschberg, B., Bond, C.T., Kinzie, J.M., Marrion, N.V., Maylie, J., and Adelman, J.P.** (1996). Small-conductance, calcium-activated potassium channels from mammalian brain. *Science* **273**: 1709–1714.
- Kosuta, S., Hazledine, S., Sun, J., Miwa, H., Morris, R.J., Downie, J.A., and Oldroyd, G.E.D.** (2008). Differential and chaotic calcium signatures in the symbiosis signaling pathway of legumes. *Proc. Natl. Acad. Sci. USA* **105**: 9823–9828.
- Lancaster, B., and Nicoll, R.A.** (1987). Properties of two calcium-activated hyperpolarizations in rat hippocampal neurones. *J. Physiol.* **389**: 187–203.
- Limpens, E., Ramos, J., Franken, C., Raz, V., Compaan, B., Franssen, H., Bisseling, T., and Geurts, R.** (2004). RNA interference in *Agrobacterium rhizogenes*-transformed roots of *Arabidopsis* and *Medicago truncatula*. *J. Exp. Bot.* **55**: 983–992.
- Loewenstein, W.R., and Kanno, Y.** (1963). The electrical conductance and potential across the membrane of some cell nuclei. *J. Cell Biol.* **16**: 421–425.
- Maekawa, T., Kusakabe, M., Shimoda, Y., Sato, S., Tabata, S., Murooka, Y., and Hayashi, M.** (2008). Polyubiquitin promoter-based binary vectors for overexpression and gene silencing in *Lotus japonicus*. *Mol. Plant Microbe Interact.* **21**: 375–382.
- Maillet, F. et al.** (2011). Fungal lipochitooligosaccharide symbiotic signals in arbuscular mycorrhiza. *Nature* **469**: 58–63.
- Matzke, M., Weiger, T.M., Papp, I., and Matzke, A.J.** (2009). Nuclear membrane ion channels mediate root nodule development. *Trends Plant Sci.* **14**: 295–298.
- Mukherjee, A., and Ané, J.M.** (2011). Germinating spore exudates from arbuscular mycorrhizal fungi: Molecular and developmental responses in plants and their regulation by ethylene. *Mol. Plant Microbe Interact.* **24**: 260–270.
- Murray, J.D. et al.** (2011). Vapyrin, a gene essential for intracellular progression of arbuscular mycorrhizal symbiosis, is also essential for infection by rhizobia in the nodule symbiosis of *Medicago truncatula*. *Plant J.* **65**: 244–252.
- Notredame, C., Higgins, D.G., and Heringa, J.** (2000). T-Coffee: A novel method for fast and accurate multiple sequence alignment. *J. Mol. Biol.* **302**: 205–217.
- Peiter, E. et al.** (2007). The *Medicago truncatula* DMI1 protein modulates cytosolic calcium signaling. *Plant Physiol.* **145**: 192–203.
- Perry, J., Brachmann, A., Welham, T., Binder, A., Charpentier, M., Groth, M., Haage, K., Markmann, K., Wang, T.L., and Parniske, M.** (2009). TILLING in *Lotus japonicus* identified large allelic series for symbiosis genes and revealed a bias in functionally defective ethyl methanesulfonate alleles toward glycine replacements. *Plant Physiol.* **151**: 1281–1291.
- Riely, B.K., He, H., Venkateshwaran, M., Sarma, B., Schraiber, J., Ané, J.M., and Cook, D.R.** (2011). Identification of legume RopGEF gene families and characterization of a *Medicago truncatula* RopGEF mediating polar growth of root hairs. *Plant J.* **65**: 230–243.
- Riely, B.K., Loughnon, G., Ané, J.M., and Cook, D.R.** (2007). The symbiotic ion channel homolog *DMI1* is localized in the nuclear membrane of *Medicago truncatula* roots. *Plant J.* **49**: 208–216.
- Riely, B.K., Mun, J.H., and Ané, J.M.** (2006). Unravelling the molecular basis for symbiotic signal transduction in legumes. *Mol. Plant Pathol.* **7**: 197–207.
- Sackin, H., Nanazashvili, M., Palmer, L.G., Krambis, M., and Walters, D.E.** (2005). Structural locus of the pH gate in the Kir1.1 inward rectifier channel. *Biophys. J.* **88**: 2597–2606.
- Shang, Z.L., Ma, L.G., Zhang, H.L., He, R.R., Wang, X.C., Cui, S.J., and Sun, D.Y.** (2005). Ca²⁺ influx into lily pollen grains through a hyperpolarization-activated Ca²⁺-permeable channel which can be regulated by extracellular CaM. *Plant Cell Physiol.* **46**: 598–608.
- Sieberer, B.J., Chabaud, M., Timmers, A.C., Monin, A., Fournier, J., and Barker, D.G.** (2009). A nuclear-targetedameleon demonstrates intranuclear Ca²⁺ spiking in *Medicago truncatula* root hairs in response to rhizobial nodulation factors. *Plant Physiol.* **151**: 1197–1206.
- Tadege, M., Ratet, P., and Mysore, K.S.** (2005). Insertional mutagenesis: A Swiss Army knife for functional genomics of *Medicago truncatula*. *Trends Plant Sci.* **10**: 229–235.
- Tadege, M., Wen, J., He, J., Tu, H., Kwak, Y., Eschstruth, A., Cayrel, A., Endre, G., Zhao, P.X., Chabaud, M., Ratet, P., and Mysore, K.S.** (2008). Large-scale insertional mutagenesis using the *Tnt1* retrotransposon in the model legume *Medicago truncatula*. *Plant J.* **54**: 335–347.
- Thion, L., Mazars, C., Nacry, P., Bouchez, D., Moreau, M., Ranjeva, R., and Thuleau, P.** (1998). Plasma membrane depolarization-activated calcium channels, stimulated by microtubule-depolymerizing drugs in wild-type *Arabidopsis thaliana* protoplasts, display constitutively large activities and a longer half-life in ton 2 mutant cells affected in the organization of cortical microtubules. *Plant J.* **13**: 603–610.
- Thuleau, P., Moreau, M., Schroeder, J.I., and Ranjeva, R.** (1994). Recruitment of plasma membrane voltage-dependent calcium-permeable channels in carrot cells. *EMBO J.* **13**: 5843–5847.
- Venkateshwaran, M., and Ané, J.M.** (2011). Legumes and nitrogen fixation: Physiological, molecular, evolutionary perspective and applications. In *The Molecular Basis of Nutrient Use Efficiency in Crops*, M. Hawkesford and P. Barraclough, eds (Oxford, UK: Wiley-Blackwell), pp. 443–489.
- Wais R.J., Galera C., Oldroyd G., Catoira R., Penmetza R.V., Cook D., Gough C., Dénarié J., and Long S.R.** (2000). Genetic analysis of calcium spiking responses in nodulation mutants of

- Medicago truncatula*. Proc. Natl. Acad. Sci. USA **97**: 13407–13412.
- Wais, R.J., Keating, D.H., and Long, S.R.** (2002). Structure-function analysis of nod factor-induced root hair calcium spiking in Rhizobium-legume symbiosis. Plant Physiol. **129**: 211–224.
- Wang, B., Yeun, L.H., Xue, J.Y., Liu, Y., Ané, J.M., and Qiu, Y.L.** (2010). Presence of three mycorrhizal genes in the common ancestor of land plants suggests a key role of mycorrhizas in the colonization of land by plants. New Phytol. **186**: 514–525.
- Wojciechowski M.F., Lavin M., and Sanderson M.J.** (2004). A phylogeny of legumes (Leguminosae) based on analysis of the plastid matK gene resolves many well-supported subclades within the family. Am. J. Bot. **91**: 1846–1862.
- Yamashita, M.** (2011). Fluctuations in nuclear envelope's potential mediate synchronization of early neural activity. Biochem. Biophys. Res. Commun. **406**: 107–111.
- Ye, S., Li, Y., and Jiang, Y.** (2010). Novel insights into K⁺ selectivity from high-resolution structures of an open K⁺ channel pore. Nat. Struct. Mol. Biol. **17**: 1019–1023.
- Zhu, H., Riely, B.K., Burns, N.J., and Ané, J.M.** (2006). Tracing nonlegume orthologs of legume genes required for nodulation and arbuscular mycorrhizal symbioses. Genetics **172**: 2491–2499.